

See discussions, stats, and author profiles for this publication at: <https://www.researchgate.net/publication/377748535>

Acoustic properties of natural fiber reinforced composite micro-perforated panel (NFRC-MPP) made from cork fiber and polylactic acid (PLA) using 3D printing

Article in *Journal of Building Engineering* · May 2024

DOI: 10.1016/j.jobe.2024.108491

CITATIONS

0

READS

30

6 authors, including:



Ebrahim Taban

Mashhad University of Medical Sciences

65 PUBLICATIONS 1,109 CITATIONS

[SEE PROFILE](#)



Umberto Berardi

403 PUBLICATIONS 14,096 CITATIONS

[SEE PROFILE](#)



Mohammad Faridan

Lorestan University of Medical Sciences

39 PUBLICATIONS 618 CITATIONS

[SEE PROFILE](#)

Contents lists available at [ScienceDirect](https://www.sciencedirect.com)

Journal of Building Engineering

journal homepage: www.elsevier.com/locate/job

Acoustic properties of natural fiber reinforced composite micro-perforated panel (NFRC-MPP) made from cork fiber and polylactic acid (PLA) using 3D printing

Ehsan Rezaieyan^a, Ebrahim Taban^{b,*,**}, Umberto Berardi^{c,*},
Seyyed Bagher Mortazavi^a, Mohammad Faridan^d, Elham Mahmoudi^a

^a Department of Occupational Health Engineering, Faculty of Medical Sciences, Tarbiat Modares University, Tehran, Iran

^b Department of Occupational Health Engineering, School of Health, Mashhad University of Medical Sciences, Mashhad, Iran

^c Toronto Metropolitan University, 350 Victoria St, Toronto, ON M5B 2K3, Canada

^d Environmental Health Research Center, Department of Occupational Health and Safety at Work Engineering, Lorestan University of Medical Sciences, Khorramabad, Iran

ARTICLE INFO

Keywords:

Sound absorption coefficient

Microperforated panel absorber

3D printing

Natural fibre-reinforced composites (NFRCs)

ABSTRACT

The present study investigated the acoustic performance of biodegradable MPP absorbers made of natural fiber-reinforced composites (NFRC) using 3D printing. The novelty of this current research lies in the recent development of a methodology that aids industry professionals in optimizing the production of MPP (Micro-Perforated Panel) at a competitive cost. This is achieved by addressing and eliminating various issues commonly faced in traditional manufacturing processes, such as manual preparation and pressing. The FDM technique was used to fabricate test samples utilizing the PLA/corkwood composite. Using an impedance tube device with two microphones, the acoustic absorption coefficients of MPPs with different perforation diameters, thicknesses, and perforation rates were measured. Maa's analytical model was used to predict the acoustic absorption performance. Moreover, considering the average sound absorption and total cost of fabricating the samples, RSM-CCD was employed to optimize these samples. In the end, the parallel arrangement of MPP double layer and the combination of MPP with kenaf porous material were tested in order to improve the sound absorption performance. The results showed that the average sound absorption coefficient of the NFRC-MPP sound absorber is 25 % more than that of conventional MPP sound absorbers. The sample with a perforation diameter of 0.70 mm, a panel thickness of 0.90 mm, and an 8 mm distance between the perforations was selected as the optimal sound absorber. The measurement and model data for NFRC-MPP panels do not correspond well. The parallel arrangement of two layers of MPP and the addition of an optimized kenaf layer behind the MPP significantly improved the sound absorption performance in the intended frequency range. The findings of this study, coupled with data available in the literature for other types of biocomposite Micro-Perforated Panel (MPP), strongly indicate that Cork fiber-based MPP exhibits substantial promise for application, either independently or in conjunction with Kenaf materials, as a material for acoustic conditioning. Implementing smart manufacturing techniques for acoustic panels not only enhances engineering noise control efforts but also amplifies the overall effectiveness of Hearing Conservation Programs.

* Corresponding author

** Corresponding author.

E-mail addresses: Tabane@mums.ac.ir (E. Taban), uberardi@torontomu.ca (U. Berardi).

<https://doi.org/10.1016/j.job.2024.108491>

Received 21 April 2023; Received in revised form 3 January 2024; Accepted 7 January 2024

Available online 9 January 2024

2352-7102/© 2024 The Author(s).

Published by Elsevier Ltd.

This is an open access article under the CC BY license

(<http://creativecommons.org/licenses/by/4.0/>).

1. Introduction

Frequent exposure to excessive noise levels may contribute to many health-related adverse consequences such as lack of relaxation, cognitive impairment, sleep disruption, cardiovascular disorders, hypertension as well as other related conditions [1–3]. Therefore, straightforward and efficient engineering techniques for noise control have been widely developed over the previous decades. Absorption of the sound energy along its propagation route via micro-perforated panels (MPPs) is considered one such technique [4,5]. MPPs are the new generation of resonant absorbers; they consist of thin plates with sub-millimeter perforations and thicknesses less than 1 mm and are mostly constructed of insulating materials such as metal or plastic. This type of absorber, initially described by Maa, has a comparatively simple structure [6]. MPPs are a suitable alternative for applications in harsh environments with high temperature, humidity, and pressure such as inside the mufflers [7], ventilation ducts [8,9], sound chambers of noisy engines [10], and even swimming pools [11]. MPPs might also be employed with convenience in sanitary facilities and equipment as well as clean surroundings including hospitals, restaurants, clean rooms, and sensitive sectors such as the electronics, pharmaceutical, and food industries [12].

The optical and aesthetic features of MPP sound absorbers are also significantly important; as they can be manufactured from various types of solid and rigid materials (of varying materials, colors, sizes, and shapes), and therefore add visual appeal to the interior spaces of buildings in addition to their primary functions [13,14]. Additionally, the utilization of MPPs in conjunction with porous materials is an established and efficient approach for enhancing sound absorption coefficients at low frequencies. This method has been reported to be superior to the use of bulky multilayers of porous/fibrous sound absorbers [15]. Despite the significant benefits of MPP sound absorbers, the geometrical design and construction of an ideal MPP, while simultaneously optimizing its manufacturing costs is rather difficult. Moreover, the fabrication of MPP sound absorbers from alternate media, such as fibrous/porous biodegradable materials with high mechanical resistance and no fiber release, has proven to be challenging in practice.

Given that the sustainability, economic efficiency, and competitive advantage of products are of particular importance in today's global marketplace [16], previous research has proposed a variety of techniques to boost the economic efficiency of fabricating MPP sound absorbers. For instance, a variety of approaches and techniques such as drilling with a hand drill [17], mechanical drilling [18], laser drilling [19], infiltration [20], along with using porous ceramic materials [21], microfiltration [22], ultra-micro perforations based on microelectromechanical systems (MEMS) [23]; and recently, the 3D printing technique for fast and cost-effective fabrication of MPPs have been reported in the literature [24]. Additive manufacturing (AM), also known as 3D printing, is the technique for layer-by-layer construction of a 3D object through computer-aided design. AM is now considered one of the pillars of sustainable industry 4.0 and has a significant contribution owing to the one-of-a-kind benefits it offers [25]. This method makes it feasible to produce sound absorbers with customized acoustic properties [26] as well as mass-producing acoustic absorbers of virtually any shape and size, while also avoiding the downsides associated with traditional manufacturing processes such as higher cost, time-consuming processes, and environmental impacts [27]. The most recent applications of this technology in the field of acoustics are the fabrication of resonators [28,29], sonic crystals [30–32], ceramic micro lattices [33], space-coiling structures [34–36], and micro perforated panels [37–40]. In general, it is the frequency range of the sound and the resolution of the manufacturing process which determine the printing technique most suited for fabricating the acoustic absorbers [41]. For instance, fused deposition modeling (FDM), one of the most extensively used 3D printing approaches, is one of the most frequent techniques utilized for low-frequency acoustic applications [37,42]. With this technique, the feature of sound absorption may be regulated by adjusting the printing parameters, such as the filament diameter, the distance between filaments, and the filament orientation [43].

Recent years have seen a shift away from using synthetic fibers in favour of natural fibers in the 3D printing of composites due to concerns over carbon footprint throughout the product's life cycle and an increased appreciation for the versatility of composites fabricated from natural fibre [44]. Stoof et al. were among the pioneering researchers who employed FDM and 3D printing to fabricate natural fibre-reinforced composites (NFRCs) Component with filaments of both hemp and harakeke with polylactic acid (PLA). According to the results from this study, uniform 3-mm filaments were successfully produced and allowed for printing tensile test samples [45]. 3D printing of NFRCs provides an opportunity to mass-produce customized acoustic absorbers while reducing wasteful use of raw materials and economizing on production time and expense; hence producing acoustic absorbers with enhanced mechanical resistance and acoustic performance [43]. Sekar et al. were the very first authors who utilized 3D printing technique to study the effect of perforation volume on acoustic absorption of MPPs fabricated from PLA polymer reinforced with wood fibers [46]. They discovered that changing the perforation volume would impact the MPP's ability to absorb sound, with MPP having a thickness of 2 mm and a perforation diameter of 0.2 mm show a maximum sound absorption coefficient of 0.93 at 2173 Hz.

Nonetheless, several disadvantages have been attributed to the use of NFRCs; such as their vulnerability to microbial growth [47], poor mechanical properties [48], dispersion of fibers from the surface, and limited resilience to heat and flame [49]. These issues would, however, be resolved through the selection of appropriate filament manufacturing techniques (e.g. dry, wet, melt and gel spinning) as well as the optimization of filament parameters (e.g. fiber geometry, fiber content, treatment of fiber, and fiber morphology), process parameters (e.g. nozzle diameter, filament diameter, printing speed, melting temperature, infill geometry, infill thickness, number of layers, and thickness of layers), and environmental conditions (e.g. the humidity of the fiber) [44]. The progress of manufacturing MPP is summarized in Fig. 1.

In the present work, the feasibility of producing an optimum micro perforated sound absorber from a biodegradable polylactic acid composite reinforced with cork fibres (PLA/Corkwood) was studied using 3D printing technology. The response surface method (RSM) was employed to optimize the effect of total manufacturing cost (TMC) and several parameters including perforation diameter, panel thickness, and perforation ratio on the sound absorption coefficient average (SACA) in the middle and low frequency ranges. Using an acoustic impedance tube and a two-microphone impedance technique, the SACA of samples was measured experimentally in an

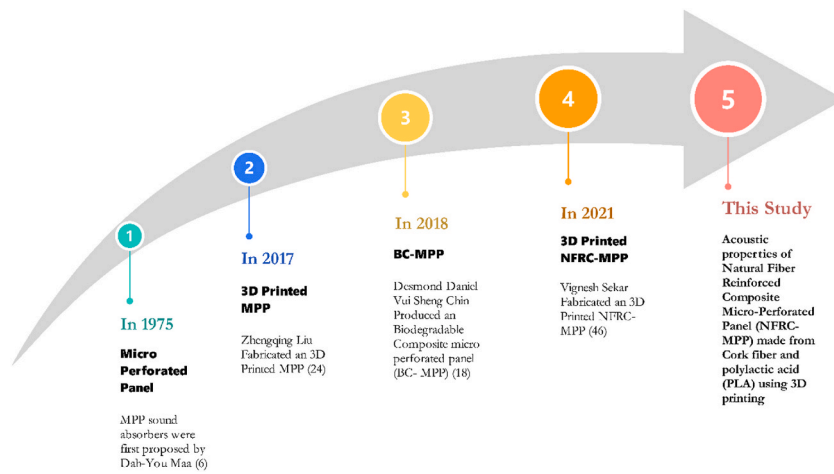


Fig. 1. Progression from initial MPP to 3D Printed NFRC-MPP.



Fig. 2. Schematic view of the stages of the study.

anechoic chamber. The Maa model was then used to predict the sound absorption characteristics of the samples. Finally, in order to improve the overall performance of the sound absorption, the combination of optimized MPP parallel arrangement with an optimized kenaf porous panel was tested.

2. Materials

The primary procedures for conducting the experiments are depicted in Fig. 2.

Table 1
Physical and mechanical characteristics of filaments.

Properties	Filament type			
	Ingeo™ Biopolymer 4043D		EasyCork™	
Physical Properties	value	Test Method	value	Test Method
Specific gravity, g/cc	1.24	ASTM D792	1.1	ISO1183
Melting temperature, °C	145–160	ASTM D3418	160	–
Print temperature, °C	190–230	–	210–260	–
Mechanical Properties	value	Test Method	value	Test Method
Impact strength	16 (J/m)	ASTM D256	5–6 (KJ/m131)	ISO179
Tensile strength, MPa	60	ASTM D882	19.4	ISO527
Tensile Modulus, MPa	3.6	ASTM D882	1050	ISO527
Tensile Elongation, %	6	ASTM D882	15	ISO527

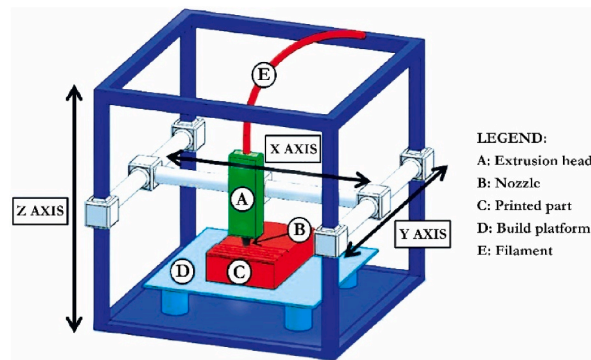


Fig. 3. Schematic representation of a typical fused deposition modeling (FDM) setup [52].

Table 2
Specification for Zortrax M200 plus [53].

Device	Material diameter	1.75 mm (0.069 in)
	Nozzle diameter	0.4 mm (0.016 in)
Printing	Technology	LPD (Layer Plastic Deposition) – depositing melted material layer by layer onto the build platform
	Layer resolution	90–390 μm
	Minimal wall thickness	450 μm
Temperature	Maximum printing temperature (extruder)	290 °C (554 °F)
	Maximum platform temperature	105 °C (221 °F)
	Ambient operation temperature	20–30 °C (68–86 °F)
	Storage temperature	0–35 °C (32–95 °F)
Software	Software bundle	Z-SUITE
	Supported file types	.stl, .obj, .dxf, .3mf, .ply

2.1. Design and fabrication of MPPs

In order to create the optimized MPP absorbers, two types of commercial filaments (PLA polymer filament and PLA/CORKWOOD composite filament), were used so that the acoustic absorption effect of the fibers in NFRC-MPP samples could be precisely monitored. PLA is a thermoplastic aliphatic polyester derived from fermented plant starch from rice, maize, corn, sugarcane, or sugar beet pulp. The standard PLA filament used in this study was Ingeo™ Biopolymer 4043D manufactured by Nature Work. Commercial corkwood filaments (EasyCork™ by Form Futura®) were also employed to 3D print the NFRC-MPPs. The EasyCork™ filaments were a light-weight polymer containing 30 wt% natural cork fibres and 70 wt% biodegradable PLA polymer. They, therefore, had features remarkably comparable to corkwood and shared many of the same properties, including being lightweight and having a high resistance to impact. Both filaments had also a standard diameter of 1.75 ± 0.05 mm. Table 1 displays the physical and mechanical properties listed in the technical data sheet of these filaments.

The use of cork fiber in the construction industry has a long history. This versatile material is well-suited to meet a wide range of requirements in this sector. With its unique combination of attributes, including lightness, elasticity, resilience, impermeability, insulation, wear resistance, fire retardant qualities, hypoallergenic properties, and durability, it stands out from traditional materials like wood or stone. Cork boasts a distinct biological cellular structure featuring closed cells arranged in a hexagonal honeycomb

Table 3
CCD experimental design matrix and responses for SACA and cost.

Independent variables			Range and levels (coded)				
Factors	Coded	Units	$-\alpha$	Low	Middle	High	$+\alpha$
Thickness	A	mm	0.6	0.7	0.8	0.9	1
Perforation diameter	B	mm	0.6	0.7	0.8	0.9	1
Perforation spacing	C	mm	2	4	6	8	10

std	Run order	Independent variables			Response	
		A	B	C	SACA	Cost (IRR) ^a
6	1	0.9	0.7	8	0.28	1,126,930
20	2	0.8	0.8	6	0.22	1,097,050
17	3	0.8	0.8	6	0.22	1,097,050
5	4	0.7	0.7	8	0.22	1,027,520
16	5	0.8	0.8	6	0.22	1,097,050
7	6	0.7	0.9	8	0.23	957,990
12	7	0.8	1	6	0.17	1,040,800
4	8	0.9	0.9	4	0.15	1,116,970
11	9	0.8	0.6	6	0.25	1,100,370
10	10	1	0.8	6	0.25	1,209,740
3	11	0.7	0.9	4	0.12	951,350
2	12	0.9	0.7	4	0.20	1,176,540
8	13	0.9	0.9	8	0.25	1,123,610
19	14	0.8	0.8	6	0.22	1,097,050
15	15	0.8	0.8	6	0.22	1,097,050
13	16	0.8	0.8	2	0.06	1,063,850
14	17	0.8	0.8	10	0.27	1,100,370
9	18	0.6	0.8	6	0.19	928,110
18	19	0.8	0.8	6	0.22	1,097,050
1	20	0.7	0.7	4	0.17	1,020,880

The test of analysis of variance (ANOVA), as well as descriptive statistics such as degree of freedom (DoF), mean square, F-value, standard deviation (SD), correlation coefficient (R^2), adjusted correlation coefficient (R^2_{adj}), and the sum of squares of predicted residuals (PRESS) were used to analyze the statistical significance of the model.

^a Official currency of Iran.

pattern, resembling stacked layers like bricks. This exceptional structural composition makes it an ideal choice for both thermal and acoustical insulation applications [50,51]. Surprisingly, the exploration of its acoustic properties has received limited attention.

2.2. 3D printing

All the samples were fabricated by printing PLA and PLA/corkwood materials on fixed bed via a FDM 3D printer (Zortrax, Poland, model M200 plus) with the resolution 0.09–0.39 mm per layer (Fig. 3). The nozzle temperature was fixed at 210 °C and 230 °C for IngeoTM Biopolymer 4043D and EasyCork respectively. The ambient temperature was around 22 °C.

First, the samples were designed according to the specifications provided by the RSM method using the AutoCAD software and with the standard file format (i.e., Standard Triangle Language/STL). All samples were 3D printed with a diameter of 100 mm at an infill density of 100 %. The specifications of the 3D printer are summarized in Table 2. NFRC-MPP and PLA-MPP samples were weighed by a laboratory scale (AND model HR 160i made in Japan) with a measurement accuracy of 0.0001 g. The obtained values of the mass of each sample were then used to determine the required filaments (g) and in turn the TMC estimation. The dimensions of the samples including their diameters and thicknesses as well as their perforation diameters and the perforation spacing (the distance between the centers of adjacent perforations) were measured by a digital calliper (INSIZE, model 1114-150 A), with a nominal accuracy of 0.03 mm. In the procedure of finishing the samples after printing (post-processing), the blocked perforations were manually drilled out with a \varnothing 0.3 mm hard alloy micro drill bit. Moreover, fine-grit sandpaper was utilized to remove extra residue from the samples' edges and backs.

More details about the construction of the samples can be found in the authors' previous study [54]. This study is an extension of that previous study.

2.3. Design of experiments (DoE)

RSM is an attractive statistical technique for modeling and optimizing parameters affecting the acoustic performance of acoustic absorbers [55]. Using the RSM technique and the five-level- three -factor central composite design (CCD) methodology, the experimental design was determined in order to achieve the highest values of SACA and the lowest possible cost (as the two predicted responses). The method uses mathematical and statistical techniques to analyze and optimize a process in which a response of interest (SACA, Cost) is influenced by several independent variables (i.e. d, t, b). Each quantitative variable is calculated at five levels in the CCD method, including axial points (levels $\pm \alpha$) and central level (0) in the middle of the minimum (-1) and maximum ($+1$) values (Table 3). The results were then fitted into a quadratic model, Eq. (1) using Design Expert 12 (Stat-Ease Inc, USA):

Table 4
Breakdown of items included in the Estimation of the cost of 3D printed MPP.

Cost item	Estimation formula ^b
Filament Cost (FC)	$FC_i(IRR) = M_i(gr) \times P(IRR/gr)$
Designing Cost (DC)	$DC_i(IRR) = DT_i(hr) \times W(IRR/hr)$
Printing Cost (PC)	$PC_i(IRR) = PT_i(hr) \times K(IRR/hr)$
Post-processing Cost (PPC) ^a	$PPC_i(IRR) = PC_i/4$
Total Manufacturing Cost (TMC)	$TMC_i(IRR) = FC_i(IRR) + DC_i(IRR) + PC_i(IRR) + PPC_i(IRR)$

^a Post-processing is an essential process in additive manufacturing. In this final stage of the manufacturing process, items are given finishing touches such as smoothing and cleaning.

^b M_i : mass of filament used for each panel in grams, P : market price per gram of filament in Rial (IRR), DT_i : labor time on designing CAD model in hour, W : average hourly earnings for The Graphic designer in Rial (IRR), K : average hourly 3D printing service fee in Rial (IRR), PT_i : time spend on printing specimens in hour.

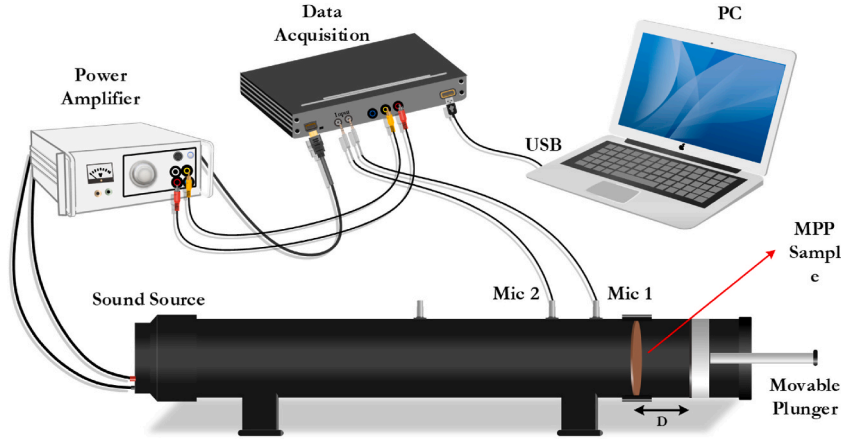


Fig. 4. Schematic view of the two-microphone impedance tube system.

$$R = A_0 + \sum_{i=1}^k A_i X_i + \sum_{i=1}^k A_{ii} X_i^2 + \sum_{i=1}^{k-1} \sum_{j=2}^k A_{ij} X_i X_j + \epsilon \quad (1a)$$

where R (response) is either the value of SACA or Cost; X_k, \dots, X_j, X_i are the input parameters (i.e. diameter of the perforation, panel thickness, the distance between perforations); A_0 is the intercept; A_i ($i = 1, 2, \dots, k$) is the linear effect, A_{ii} ($i = 1, 2, \dots, k$) is the squared effect, A_{ij} ($i = 1, 2, \dots, k-1, j = 1, 2, \dots, k$) is the interaction effect and ϵ is the statistical error.

Numerical optimization involves exploring the design space by utilizing the models developed during the analysis to identify factor settings that align with predefined objectives. To determine the optimal set of variables, we employed a method that prioritizes responses based on SACA and cost considerations. In this study, we prioritized increasing SACA values over reducing costs. The software's output was evaluated using a 5-point scale to assess the relative importance of responses. The perceived "importance" of a particular goal can be adjusted in relation to other objectives. To this end, a scale of 5 was assigned to SACA, while a scale of 1 was assigned to cost. In order to perform simultaneous optimization, each response must be assigned low and high values for each goal. If a goal is not applicable, the response will not be utilized for the optimization process. Numerical Optimization is capable of optimizing any combination of one or more objectives. The goals pertinent to SACA and Cost are respectively "Maximize" and "Minimize." This implies that the lower limit for SACA represents the minimum acceptable outcome, while the upper limit signifies the desired optimal result. For Cost, the lower limit indicates the desired optimal result, and the upper limit represents the highest acceptable outcome. Confirmation testing is intended to validate the model's ability to predict actual outcomes using the optimal settings determined through the analysis. In this respect, five samples were fabricated and tested at the identified optimal point.

2.4. Estimation of the cost

In the present research, the concept of cost estimation is considered as the process of the design and development from ideation to the manufacturing of a functional lab-scale prototype. It is worth noting that this process would never include the product's final selling price. Also, no remarks will be made regarding the profitability of the product. It is, however, difficult to accurately estimate the cost of applying the proposed sound absorber in a real environment. Nonetheless, by calculating the cost of fabricating a lab-scale sample or prototype, it would be possible to estimate the cost of developing a full-scale sound absorber through establishing a reasonable ratio. To establish the total cost of fabricating each sample, it was necessary to combine together the costs and expenses of purchasing the filaments, designing, 3D printing, and overall payments. Table 4 demonstrates the details of the costs and expenses associated with each item.

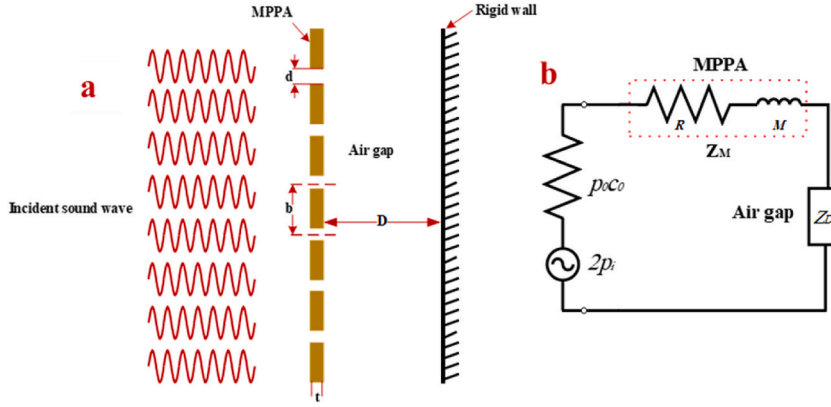


Fig. 5. a) Schematic diagram of single layer MPP sound absorber. b) the equivalent electroacoustic circuit analogy.

2.5. Sound absorption measurement

The normal incidence sound absorption coefficient of the samples was measured with a two-microphone acoustic impedance tube system (SW420-470, BSWA TECH) in accordance with ISO 10534–2. Fig. 4 depicts the schematic representation of how the SACs of the samples were determined in the acoustics lab. The impedance tube system included 2 MPA416 1/4-inch microphones compliant with the IEC61672 (Class 1) standard, a speaker, a digital frequency measuring system, a tube, a PA50 amplifier, 2 MPA416 1/4-inch microphones, and several auxiliary components. BSWA VA-Lab4 Basic software was also employed for data processing. Prior to each measurement, the microphones were calibrated by means of a CA115 calibrator at a frequency of 1 kHz and a sound pressure level of 114 dB. Two tubes with internal diameters of 30 mm and 100 mm, were respectively used to measure the SACs at higher (1000–6300 Hz) and lower (range 63–1600 Hz), frequency ranges. The samples were positioned within the larger tube on the rigid surface with precision and accuracy. Having securely positioned each sample and verified that its edge aligned with the tube wall, the desired back cavity (i.e. air gap) was created at its back by sliding (adjusting) the plunger. Sound absorption measurements were repeated 3 times for each sample and the average values were reported. In order to minimize the possible errors due to the incorrect placement of the sample inside the tube, for each measurement, the sample was removed from the tube and reinserted again. All measurements were carried out under controlled temperature conditions of 20 ± 2 °C, relative humidity of 10 ± 45 %, and a pressure value of $101,325 \times 105$ Pa.

After data measurement, the acoustic absorptivity of materials is judged by their SACs. The Sound Absorption Coefficient Average (SACA) is defined as the arithmetic mean of the sound absorption coefficients in the 1/3 octa band central frequencies in the frequency range of 63–1600 Hz, as follows:

$$SACA = \frac{1}{15} \sum_{i=63\text{Hz}}^{i=1600\text{Hz}} \alpha_{fi} \quad (1b)$$

2.6. Sound absorption modeling

The theoretical analysis of the MPP absorber by Maa's model was carried out based on the equivalent electro-acoustic circuit (EAC) under the simplified conditions. As illustrated in Fig. 5, a single MPP layer is positioned at a distance D from a rigid wall. Taking into account EAC analogy, the acoustic impedance, the pressure difference, and the particle velocity correspond to the electric impedance, the voltage, and the electric current, respectively. Included in the equivalent EAC are the values R and M , which stand in for the perforations' specific acoustic resistance and specific acoustic reactance.

The basic structure and the theory of the micro-perforated panel (MPP) absorber was first proposed by Maa [56,57]. The central concept of Maa's theory is to view the MPP as a parallel connection of the perforations; hence, in this case, the perforation would be viewed as a short narrow tube. Propagation of sound waves through the short tubes (perforations) was first modeled by Rayleigh, and a simplified version was provided by Crandall for tubes that are extremely short relative to the wavelength and taking into account the viscous effect inside these short tubes. In case of perforated panels, end correction should be applied to the real and imaginary part of the transfer impedance. Taking into account the discontinuity between the equations proposed by Crandall, Maa developed an approximate solution for sub-millimeter-sized perforations (i.e. the MPPs).

According to Maa [6], the relative acoustic impedance z_m of MPP (normalized by $\rho_0 c_0$) considering the theoretical formula developed by Maa including the impedance of the MPPA layer and the end corrections is given by

$$Z_{MPP} = (R + jM) / \rho_0 c_0 = r + j\omega m \quad (2)$$

where r is the normalized specific acoustic resistance and given by

$$r = \frac{32\eta t}{\rho \rho_0 c_0 d^2} \left(\sqrt{1 + \frac{x^2}{32}} + \frac{\sqrt{2}}{8} \frac{xd}{t} \right) \quad (3)$$

Table 5
The summary of structural and acoustic absorption characteristics of the fabricated samples.

Sample number	Material	Specimen diameter, (mm)	Specimen Thickness, t (mm)	Perforation diameter, d (mm)	Perforation spacing, b (mm)	Perforation ratio, p (%)	SACA		
							Back cavity 30	Back cavity 50	Back cavity 70
SL-MPP 1	PLA/ Corkwood	100.2	0.6	0.8	6	1.40	0.16	0.19	0.20
SL-MPP 2	PLA/ Corkwood	100.1	0.7	0.7	4	2.40	0.14	0.17	0.18
SL-MPP 3	PLA/ Corkwood	100.3	0.7	0.7	8	0.60	0.21	0.22	0.23
SL-MPP 4	PLA/ Corkwood	100.1	0.7	0.9	4	3.97	0.09	0.12	0.12
SL-MPP 5	PLA/ Corkwood	100.0	0.7	0.9	8	0.99	0.21	0.23	0.25
SL-MPP 6	PLA/ Corkwood	100.2	0.8	0.6	6	0.79	0.22	0.25	0.26
SL-MPP 7	PLA/ Corkwood	100.1	0.8	0.8	2	12.56	0.04	0.06	0.06
SL-MPP 8	PLA/ Corkwood	100.3	0.8	0.8	6	1.40	0.19	0.22	0.23
SL-MPP 9	PLA/ Corkwood	100.1	0.8	0.8	10	0.50	0.25	0.27	0.29
SL-MPP 10	PLA/ Corkwood	100.2	0.8	1	6	2.18	0.15	0.17	0.17
SL-MPP 11	PLA/ Corkwood	100.0	0.9	0.7	4	2.40	0.16	0.20	0.21
SL-MPP 12	PLA/ Corkwood	100.1	0.9	0.7	8	0.60	0.25	0.28	0.31
SL-MPP 13	PLA/ Corkwood	100.3	0.9	0.9	4	3.97	0.13	0.15	0.16
SL-MPP 14	PLA/ Corkwood	100.4	0.9	0.9	8	0.99	0.23	0.25	0.26
SL-MPP 15	PLA/ Corkwood	100.3	1	0.8	6	1.40	0.22	0.25	0.26

and m is the normalized specific acoustic reactance and given by

$$m = \frac{t}{pc_0} \left(1 + 1 \sqrt{9 + \frac{x^2}{2} + 0.85 \frac{d}{t}} \right) \quad (4)$$

and x is the perforation constant. Which is the ratio of radius to the thickness of viscous boundary layer inside the hole and given by

$$x = \frac{d}{2} \sqrt{\omega \rho_0 / \eta} \quad (5)$$

where $\omega = 2\pi f$ is the angular frequency of the incident acoustic wave, ρ_0 is the mass density of air, η is the coefficient of the kinematic viscosity of air, c_0 is the speed of sound in air. t , d , p are the thickness, hole diameter, and perforation ratio of an MPPA layer, respectively.

The perforation ratio, commonly known as the open area ratio, is the proportion of the open area to the total surface area of the panel. The perforation ratio depends on the shape of the perforations and the shape of the panel and is calculated through the following equation:

$$p = \frac{\text{Open surface}}{\text{Total surface}} \quad (6)$$

Typically, the distance between the perforations on the MPPs is smaller than the wave-length of sound in the frequency band of absorption. In case the circular perforations are evenly distributed and set at equal distances from each other (i.e. regular pattern), we would have:

$$p (\%) = \left(\frac{\pi}{4} \right) \left(\frac{d}{b} \right)^2 \times 100 \quad (7)$$

where d is the hole diameter and b is the center-to-center distance of the adjacent perforations.

The specific acoustic impedance of the air cavity, normalized by $\rho_0 c_0$ is given by

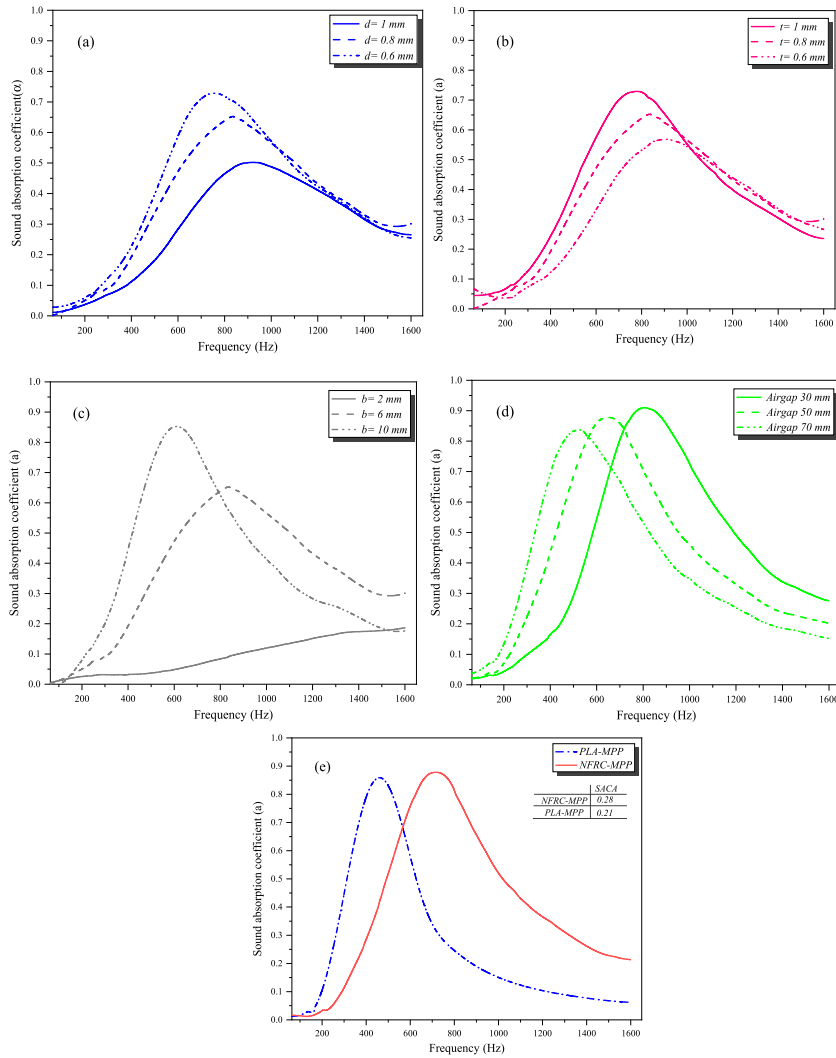


Fig. 6. The effect of parameters d, b, t, D and the panel material on the average sound absorption coefficient of NFRC-MPP absorber.

$$Z_D = -j \cot\left(\frac{\omega D}{c}\right) \tag{8}$$

According to the equivalent EAC presented in Fig. 5, the acoustic impedance for the MPP and the air cavity are in series with each other, therefore, the normalized characteristic acoustic impedance of the whole structure is calculated through the following equation:

$$z_{total} = z_{MPP} + z_D = r + j(\omega m - \cot(\omega D / c_0)) \tag{9}$$

The normal sound absorption coefficient, α_n of the MPPA layer backed by air gap are then obtained by:

$$\alpha_n = \frac{4Re(z_{total})}{[1 + Re(z_{total})]^2 + [Im(z_{total})]^2} = \frac{4r}{(1 + r)^2 + (\omega m - \cot(\omega D / c))^2} \tag{10}$$

3. Results and discussion

On the basis of the experimental design as well as applying the CCD approach, sample MPP absorbers of varying structural parameters were manufactured from PLA and PLA/Corkwood composite using 3D printing technology. According to Table 5, the maximum value of the SACA corresponds to the SL-MPP12 absorber. Table 2 also shows that sound absorption coefficient curves in most MPP samples contain identical patterns. For the majority of these samples, the sound absorption coefficient peak value is within the frequency range of 630–1250 Hz. Table 5. The summary of structural and acoustic absorption characteristics of the MPP sound absorbers.

3.1. The effect of perforation diameters

As demonstrated in Fig. 6-a, when the diameter of the perforation increased from 0.6 mm to 1 mm, the values of absorption peak and SACA reduced by 31.5 % and 32 %, respectively. Accordingly, the samples with $d = 0.6$ mm and $d = 1$ mm have the greatest values of sound absorption (i.e. 0.73 and 0.50) at 756 Hz and 922 Hz, respectively. In addition to reducing the values of peak absorption and SACA, with the increase in the diameter of the perforations, the frequency with the highest absorption shifts towards the range of higher frequencies. In contrast to the larger perforations, the smaller ones lack the acoustic resistance to absorb the sound energy, and the extent of their size also makes it more difficult for sound waves to pass through the panel. As a consequence, the majority of sound waves are reflected rather being absorbed on the MPP surface. Larger perforations boost the absorption within the high-frequency region mainly as a result of the rise in the perforation ratio and also the decrease in the total acoustic mass and the resonance frequency [58]. According to the results from the study by Qian et al. [23], the increase in the diameter of perforation from $27 \mu\text{m}$ to $80 \mu\text{m}$, would contribute to an increase in the value of the absorption peak and a decrease in the frequencies corresponding to the peaks of SACA curves. The reason underlying such an increase in the absorption peak value was the presence of extremely elevated acoustic resistance and lower acoustic mass due to smaller perforations. Larger perforations, however, contributed to an increase in the acoustic mass, which in turn caused the absorption frequency range to decrease in samples with larger perforation diameters. Drawing an analogy between a perforation and an air cavity behind that on the one hand and a Helmholtz resonator (HR) on the other hand, the increase in the diameter of the perforations in the MPP is somehow similar to the increase in the neck width of an HR, which can increase the resonance frequency of the HR, causing the SACA curve shift towards the higher frequencies [14].

3.2. The effect of thickness

As can be observed in Fig. 6-b, with the increase in the panel thickness from 0.6 to 1 mm, the peak sound absorption and SACA value have increased by 28 % and 31.6 %, respectively. The highest sound absorption values for the samples with $t = 0.6$ mm and $t = 1$ mm were 0.57 at 906 Hz and 0.73 at 778 Hz, respectively. In addition to reducing the peak values of sound absorption and SACA, the increase in the thickness of the panel makes resonance frequency shift toward the range of lower frequencies. Sakagami et al. showed that increasing the thickness of the MPP would cause the maximum sound absorption to shift towards the lower frequency range and decline the absorption coefficient values drastically. The authors would also argue that the thicker panels contributed to a significant increase in the levels of acoustic resistance and as a result, the absorption peak occurred at low frequencies [59]. Moreover, the research conducted by Usmonov et al. demonstrated that keeping the parameters d and b constant and increasing the thickness of the MPP would reduce the resonance frequency [11].

3.3. The effect of distance between the perforations

As seen in Fig. 6-c, increasing the perforation spacing from 2 to 10 mm, rendered the sound absorption peak and the SACA values increased by 347 % and 350 %, respectively. The samples with $b = 2$ mm and $b = 10$ mm showed their highest sound absorption values (i.e. 0.19 and 0.90) at 1595 Hz and 612 Hz. In addition, as the distance between the perforations increased, the frequency where the highest sound absorption occurred shifted to the higher frequency range. It is worth mentioning that in a circular panel with Constant diameter, modifying the parameters such as perforations diameter and the distance between them would also contribute to the modification of the perforation ratio. In other words, for the two identical MPPs with the same diameter (D) and circular perforation diameter (d), it is not possible to modify the distance between the perforations and simultaneously keep their perforation ratio constant. Increasing the perforation ratio of the MPP created a higher resonant frequency for the peak sound absorption coefficient; this is mainly due to the fact that such increase contributed to a decrease in the overall acoustic mass of all perforations, and thus increased the resonance frequency at which the peak sound absorption coefficient occurred [60]. As shown by Liu and colleagues [24], for the MPPs that were fabricated from VisiJet-SL polymer via SLS 3D printing, at lower frequency range, a greater sound absorption coefficient is produced by the MPP having a reduced perforation ratio. Whereas the absorption at higher frequencies may be modulated by a larger perforation ratio.

3.4. The effect of back cavity depth

As shown in Fig. 6-d, the peak values of sound absorption and SACA were selected and tested for the SL-MPP 12 sample at back cavities of 30, 50, and 70 mm. The results indicate that by extending the back cavity behind the samples from 30 to 70 mm, the maximum value of sound absorption decreased by 7.7 % and the SACA value increased by 24 %. Additionally, the increase in the length of the back cavity, made the frequency with the maximum sound absorption shift towards the lower frequency range. This discrepancy in the peak values might be due to the gradual decrease in the stiffness of the air within the back cavity. Such property is particularly useful when absorbing the sound energy is required at lower frequencies. The perforations on the panel and the air within the back cavity would respectively act as acoustic masses and acoustic springs, so a mass and spring system is created. As the back cavity depth increase, the stiffness of the spring decreases; therefore, shifting the peak absorption towards lower frequency range. When the frequency of the sound coincides with the resonance frequency, the stiffness of the spring would cause the destruction of the acoustic mass of the perforation as well as a peak in absorption [18].

3.5. The effect of material

The sound absorption performance of the MPP sound absorber made of PLA/corkwood composite compared to the MPP sound absorber made of PLA polymer in sample number 12 with a back cavity of 50 mm is illustrated in Fig. 6-e. As can be seen from the graph, NFRC-MPP outperforms PLA-MPP in terms of sound absorption thanks to its greater peak sound absorption coefficient and

Table 6
Statistical model and ANOVA for SACA.

Response	Equation	ANOVA					
		Source	Sum of square	DF	Mean square	F-value	P-value
SACA	Quadratic model $SACA = -0.232045 + 0.505682A + 0.343182B + 0.015341C - 0.5AB + 0.0125AC + 0.05BC - 0.011364A^2 - 0.261364B^2 - 0.003466C^2$	Model	0.0513	9	0.0057	77.92	<0.0001
		A-Thickness	0.0042	1	0.0042	57.73	<0.0001
		B-Perforation diameter	0.0049	1	0.0049	66.96	<0.0001
		C- Perforation spacing	0.0361	1	0.0361	493.29	<0.0001
		AB	0.0002	1	0.0002	2.73	0.1293
		AC	0.0001	1	0.0001	0.6832	0.4278
		BC	0.0008	1	0.0008	10.93	0.0079
		A2	3.247E-07	1	3.247E-07	0.0044	0.9482
		B2	0.0002	1	0.0002	2.35	0.1565
		C2	0.0048	1	0.0048	66.03	<0.0001
		Residual	0.0007	10	0.0001		
		Cor Total	0.0521				

Statistical parameters (Std. Dev = 0.0086, CV% = 4.14, Mean = 0.2065, R2 = 0.9859, R2adjusted = 0.9733, PRESS = 0.0058, Equivalent Precision = 35.14).

Table 7
Statistical model and ANOVA for cost.

Response	Equation	ANOVA					
		Source	Sum of square	DF	Mean square	F-value	P-value
Cost	Quadratic model $SCost = 1.62879 \times 10^5 + 1.53917 \times 10^5A + 1.31736 \times 10^5B + 17180.7C + 9.52125 \times 10^5AB - 35156.25AC + 35156.25BC - 8.57159 \times 10^5A^2 - 8.15659 \times 10^5B^2 - 1318.83523C^2$	Model	9.372E+10	9	1.041E+10	37.60	<0.0001
		A-Thickness	8.259E+10	1	8.259E+10	298.21	<0.0001
		B-Perforation diameter	6.444E+09	1	6.444E+09	23.27	0.0007
		C-Perforation spacing	1.175E+08	1	1.175E+08	0.4241	0.5296
		AB	7.252E+08	1	7.252E+08	2.62	0.1367
		AC	3.955E+08	1	3.955E+08	1.43	0.2597
		BC	3.955E+08	1	3.955E+08	1.43	0.2597
		A2	1.847E+09	1	1.847E+09	6.67	0.0273
		B2	1.673E+09	1	1.673E+09	6.04	0.0338
		C2	6.997E+08	1	6.997E+08	2.53	0.1430
		Residual	2.770E+09	10	2.770E+08		
		Cor Total	9.649E+10	19			

Statistical parameters (Std. Dev. = 16642.29, C.V. % = 1.55, Mean = 1.076E+06, R2 = 0.9713, R2adjusted = 0.9455, PRESS = 2.199E+10, Adeq. Precision = 2442.18).

broader absorption frequency range. Moreover, by comparing the NFRC-MPP and PLA-MPP sound absorbers, we find that the former has a peak absorption value of 0.88, while the latter reaches a value of 0.86. The difference between the values of resonance frequency for two absorbers is 189 Hz. The reason for such phenomenon could be attributed to the internal network of the pores within the NFRC-MPP samples. It has been demonstrated that an increase in the porosity correlates with an increase in the sample's sound absorption coefficient. This is because the structure of the pores can "trap" the sound waves, allowing the internal reflections of the wave and, thus, causing a loss of sound energy and sound absorption [61,62]. The previous studies have also shown that among NFRC-MPPs with the same resonant frequency and density, samples with greater interior porosity exhibited superior sound absorption [18]. According to the research by Chin Vui et al. the sound absorption performance of the MPPs fabricated from coconut fiber/PLA composite was superior to that of steel MPPs. This is particularly related to the fact that the pores and tortuous structure within MPPs were made from the coconut fibers. Conventional MPPs work by converting the kinetic energy of moving air molecules into thermal energy via friction with the surfaces of microscopic perforations, hence dampening the emitted sound. However, regarding the MPPs made of coconut fibers, in addition to the small perforations, the porous nature of these panels created by coconut fibers also has a significant effect on reducing the sound energy; thus, as the quantity of coconut fibres in the samples increases, their porosity and, subsequently, their sound absorption capability increases [63]. Other types of composites still need to be studied in the future regarding their excellent properties, including Carbon fiber-reinforced polymer composites [64], Polymer Nanocomposites [65], sandwich glass composites [66], Particle Reinforced Composites [67], Polymer ceramic composites [68], and Metal Filament [68].

3.6. Experimental design and statistical optimization

Having recorded the responses, the software provided the optimal model for our data. For both responses (i.e. SACA and cost), a quadratic polynomial equation was proposed. Tables 6 and 7 provide the anticipated equations of the model together with the results

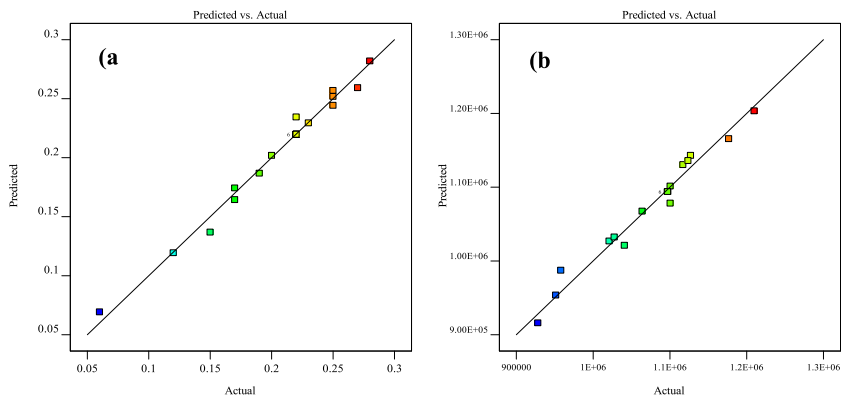


Fig. 7. The comparison between the actual and predicted values of response variables a: SACA response and b: cost response.

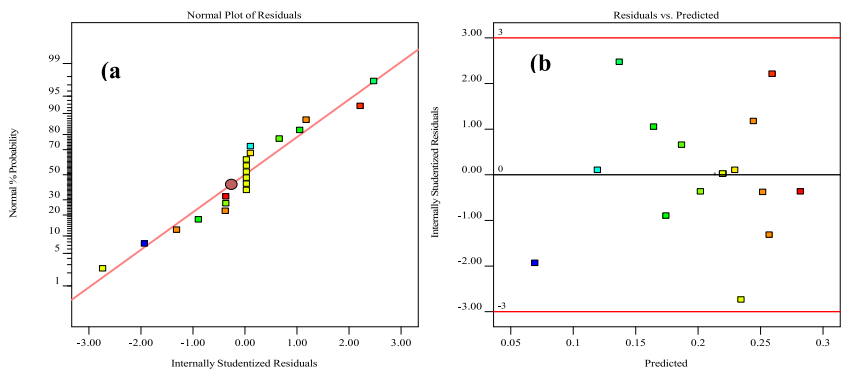


Fig. 8. a) and normal graph of residuals for the SACA response and b) Residuals vs predicted values.

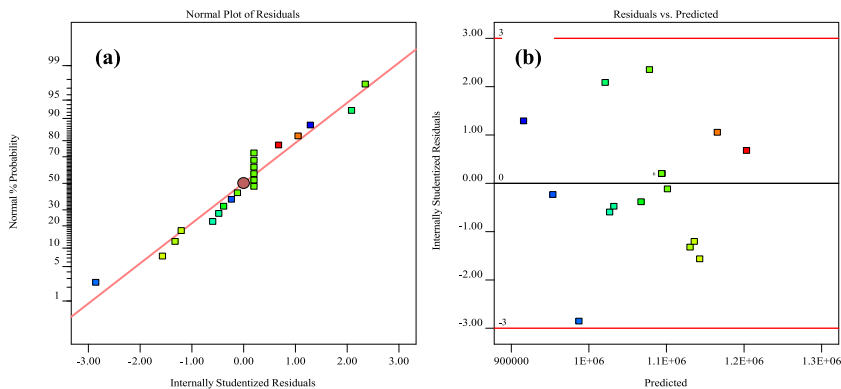


Fig. 9. a) Normal graph for residuals, and b) residuals against predicted values for the cost response (Cost).

from the ANOVA and descriptive statistics parameters, including the degree of freedom (DF), the sum of squares, the mean squares, and F and P values. Regarding the quadratic model presented for the SACA response, the F-value equal to 77.92 indicated that the model was significant. A P-value of less than 0.05 ($P < 0.05$) indicated that the terms of the model were significant as well. Considering this equation, the relevant terms for this model are the values of A, B, C, BC, and C^2 . While parameters A, B, C, and BC had a direct impact on the model parameter C^2 showed an indirect impact; Also, the coefficient of each of these parameters demonstrated that parameter A was the most effective component of the model, whilst factor C^2 was the component with the lowest level of effectiveness. Regarding the quadratic model presented for the cost response, the F-value of 37.60 indicated that the model was significant. A P-value of less than 0.05 ($P < 0.05$) was indicative of the fact that the terms of the model were also significant. Taking into account the equation, the value of A and B and A^2 and B^2 were the significant terms of this model. Values greater than 0.1 indicated that the related parameter was not considered significant in the model. Parameters A and B had a direct impact on the model and parameters A^2 and B^2 inversely

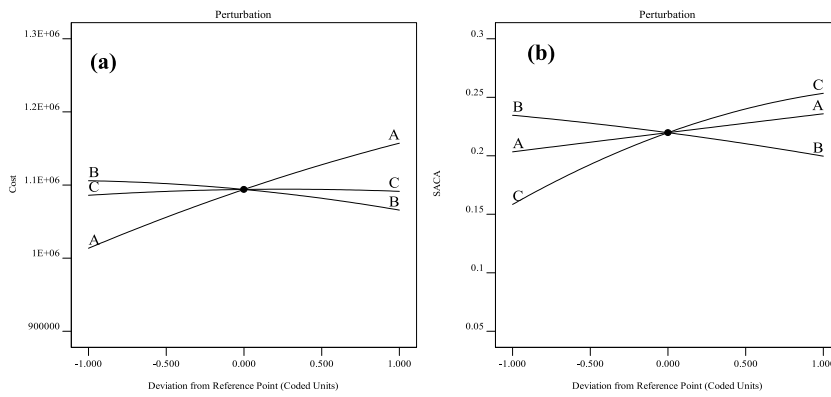


Fig. 10. Perturbation plots for response variables; (a. Cost response, and b. SACA response).

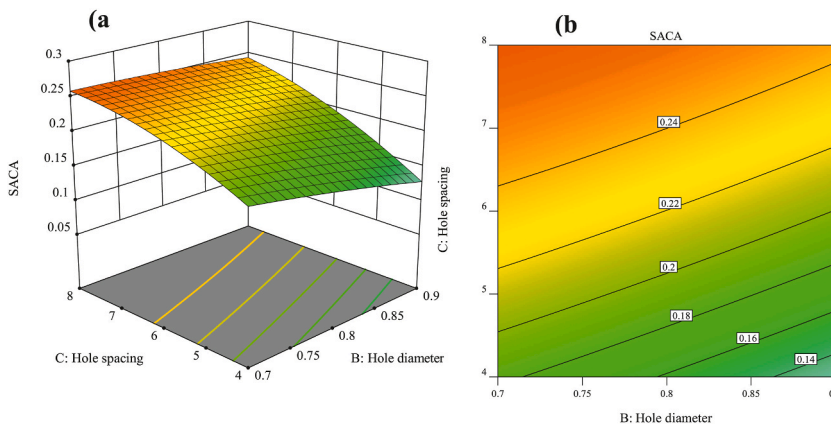


Fig. 11. Contour diagram and impact of response levels of perforation diameter (B) and perforation distance (C) on the levels of SACA while the thickness variable is at its centered point (B = 0.8 mm).

Table 8
Optimization results.

Response	Target	Importance (1–5)	Thickness (mm)	Perforation diameter (mm)	Perforation spacing (mm)	SACA	Cost (IRR)
SACA	Maximize	5	0.9	0.7	8	0.28	1,126,930
Cost	Minimize	1	0.6	0.8	6	0.19	928,110
Optimum	SACA: Max Cost: Min	SACA: 5 Cost: 1	0.87	0.7	7.99	0.275	1,131,065

impacted the regression model; Likewise, the coefficients of the equation showed that parameters A and A² were the most and the least effective components in the model. The fitness of the model was evaluated through the correlation coefficient (R²) between the experimental data and the predicted values. The R² coefficient showed what proportion of changes in the dependent variable was affected by the associated independent variable and what proportion of those changes are due to other variables. In the presented regression model the values of the R² coefficient for SACA and cost responses, were equal to 0.98 and 0.97, respectively. This indicates that the models are able to explain more than 97 % of the variability of the response data around its mean, and the proposed regression models are highly accurate. The values of the adjusted R² coefficient for SACA and cost responses were 0.97 and 0.94, respectively. There is a reasonable difference of less than 0.4 with the value of the R² coefficient, and this indicates that the model is fairly accurate and to a large extent reliable. It should be emphasised that the R² coefficient makes the assumption that each independent variable present in the model explains changes in the dependent variable; as a result, the percentage shown by this index accounts for the impact of all independent variables on the dependent variable. If the percentage indicated by the modified R² coefficient is merely the consequence of the real influence of the model’s independent variables on the dependent variable, then the coefficient should not be altered (not all independent variables). Even if the R² coefficient has a high value, it cannot assess the suitability of the variables for the model, however, the estimated value of the adjusted R² coefficient may be relied upon. Fig. 7 shows the comparison between the actual and predicted values of the two responses. The predicted and actual values have a respectable correlation, which supports the model’s resilience. Moreover, the comparison between the actual and predicted values of SACA and cost shows that the quadratic models for

Table 9

Confirmation Tests results (Confidence = 95 %).

Response	Prediction Results		Experimental Results				
	Mean	Median	Std Dev	SE Pred	n	95 % PI Low	95 % PI High
SACA	0.282	0.275	0.0085	0.0069	5	0.259	0.290
Cost	1.119E+06	1.131E+06	16642.3	13533.9	5	1.100E+06	1.161E+06

SACA ($R^2 = 0.98$) and cost ($R^2 = 0.97$) fit well.

A Model F-value of 77.92 indicates that the model is statistically significant. There is a 0.01 % probability that an F-value of this magnitude might be caused by noise. P-values less than 0.05 indicate significant model terms. Within that case, the model terms A, B, C, BC, and C^2 are mainly significant. Values over 0.1000 imply that the model terms are not statistically significant. If the model has several insignificant terms (apart from those essential to maintain hierarchy), the model reduction may be contributed to an enhancement.

The discrepancy between the Predicted R^2 value of 0.8879 and the Adjusted R^2 value of 0.9733 is less than 0.2, indicating a reasonable agreement. Signal to noise ratio is measured by Adeq Precision. A ratio larger than four is preferred. The ratio of 35.148 demonstrates a sufficient signal. This model facilitates design space navigation.

A Model F-value of 37.60 indicates that the model is statistically significant. There is a 0.01 % probability that an F-value of this magnitude might be caused by noise. P-values less than 0.05 indicate significant model terms. Within that case, the model terms A, B, A^2 , B^2 are mainly significant. Values over 0.1000 imply that the model terms are not statistically significant. If the model has several insignificant terms (apart from those essential to maintain hierarchy), the model reduction may be contributed to an enhancement.

The discrepancy between the Predicted R^2 value of 0.7721 and the Adjusted R^2 value of 0.9455 is less than 0.2, indicating a reasonable agreement. Signal to noise ratio is measured by Adeq Precision. A ratio larger than 4 is preferred. The ratio of 24.422 demonstrates a sufficient signal. This model facilitates design space navigation.

The normal distribution of the data and the equality of variances serve as the major prerequisites for the ANOVA test. In that regard, if the data is distributed normally, Fig. 8-a and 9-a ought to be approximately linear as well. The internally studentized residual is calculated by dividing the residual by the standard deviation. These two graphs show that the residuals follow a normal distribution, and except for a few fairly scattered points, all points are closely aligned on a straight line. This confirms that both of the presented models are adequately validated and can be applied successfully to the laboratory data; hence, the first precondition, namely the normal distribution of the data is established. Fig. 8-b and 9-b show that with respect to both the SACA variable and the interaction cost the points are randomly distributed.

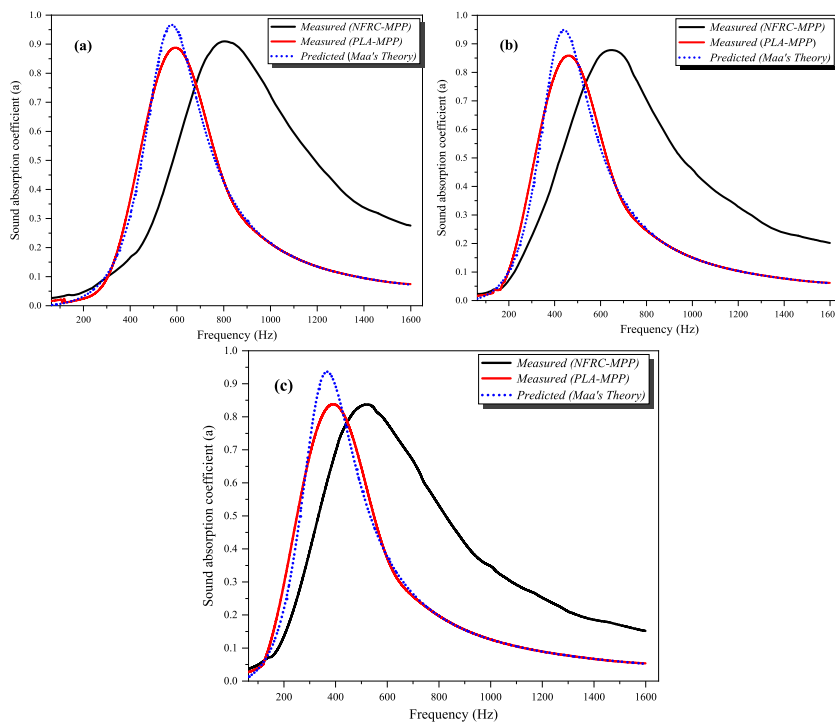


Fig. 12. Comparison between the predicted and measured sound absorption coefficients of MPP 12 made of PLA/corkwood and PLA with varying back cavities (A = 30 mm, B = 50 mm, C = 70 mm).

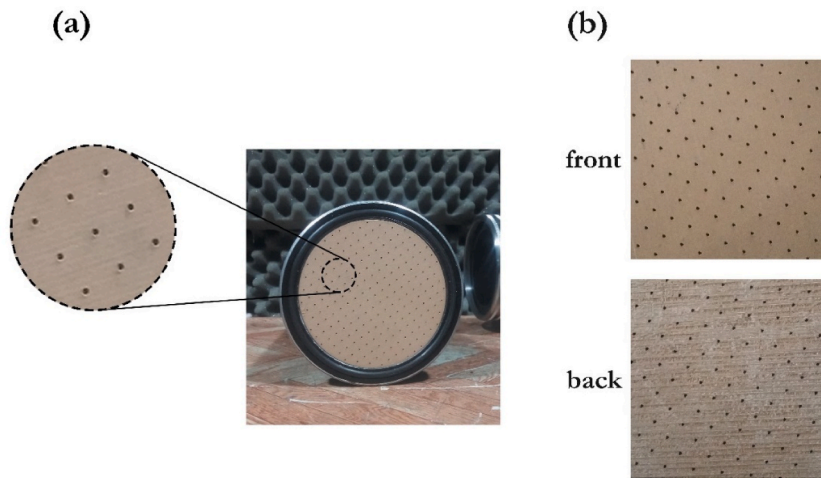


Fig. 13. a) NFRC-MPP Irregular Circular Shapes; b) front and Back surface 3D printed NFRC-MPP sound absorber.

Considering the SACA model, the accuracy rate of 35.14, which is much larger than 4, suggests a favorable signal-to-noise ratio (SNR) and indicates that the model is suitable for design purposes. The low value of the coefficient of variation ($CV = 4.14$) confirms that the tests are highly reliable. Similar results were obtained for the cost-related regression model, where the accuracy value was 24.42 and the $CV\%$ was 1.55, indicating the model's suitability. The models may thus be utilized to predict the values of SACA and the cost of MPP absorbers within the range of input variables. In other words, these models offer sufficient accuracy and reliability and can be used to fabricate such absorbers.

In order to evaluate the effects of each of the independent variables on the responses, perturbation plots are shown in Fig. 10. The perturbation plots interpret the individual effect of each independent variable on the response variable, assuming that all other variables remain constant. In this plot, the higher slope represents the higher sensitivity of the response. Therefore, the greater slope of a plot confirms its significant contribution to the response. Regarding SACA, Fig. 10-b shows that variables A and C have a positive slope, whereas variable B has a steep negative slope; it is worth noting that the value and slope direction of each of these parameters are determined by assuming that the other two parameters are constant, and these values should not be compared with the coefficients of the parameters in the regression equation. Fig. 10-a shows that variable A in the cost response has a steep positive slope, while

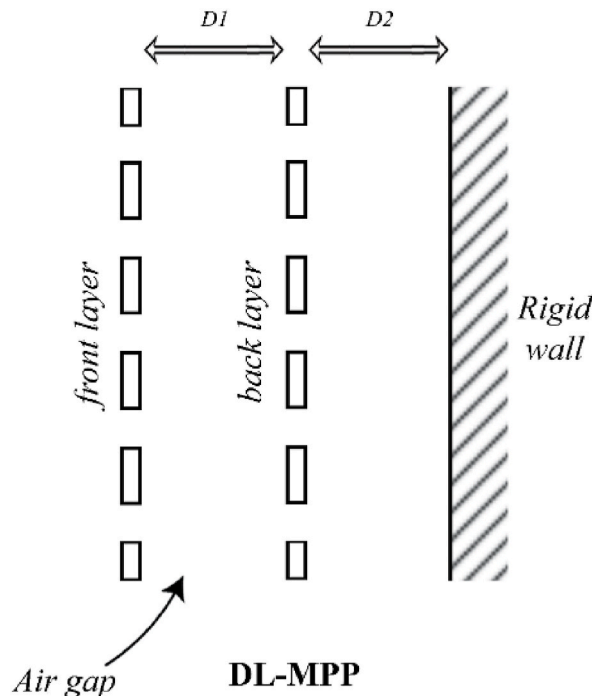


Fig. 14. Schematic illustration of DL-MPP.

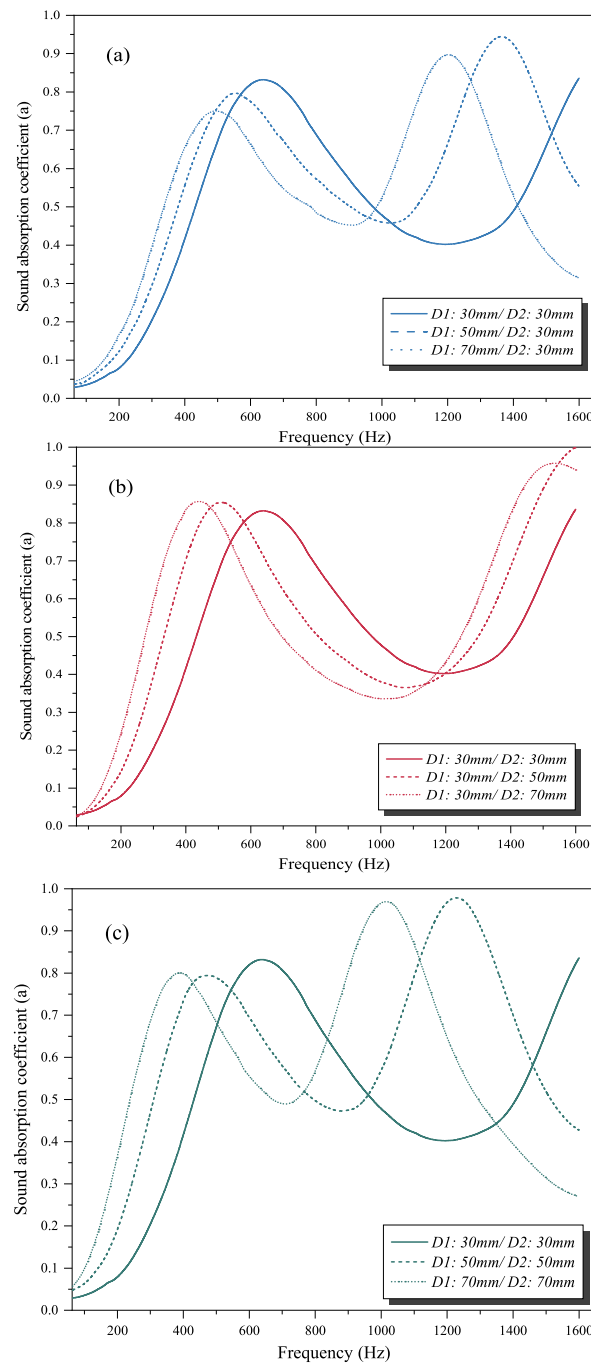


Fig. 15. The effect of back cavity modifications on the sound absorption coefficient of DL-MPP absorbers a) Increasing the depth of back cavity D1, b) Increasing the depth of back cavity D2, c) Simultaneous increase in the back cavities D1 and D2.

variables B and C have lower negative slopes. As a result, we may conclude that the influence of variable A is more significant than the effects of variables B and C.

Response surface and contour diagrams were used to examine the influence of the parameters on the optimal properties of the MPP sound absorbers and to identify the optimal circumstances for achieving the required properties. According to Fig. 11, the diameter of the perforations and the distance between them are quadratically related to the values of SACA. In other words, the values of SACA increase when the diameter of perforations decreases and the distance between them increase, and vice versa.

The optimal conditions for software outcomes (with SACA priority over cost) occurred when the values of thickness, the diameter of perforations, and the distance between perforations were equal to 0.2, 0.2, and 5, respectively (Table 8).

Table 10
The effect of changing the second layer on the absorption coefficient of DL-MPP absorbers.

Model	MPPA layer 1 (Front MPP)				MPPA layer 2 (Back MPP)				SACA	Absorption peak	
	t (mm)	d (mm)	b (mm)	D1 (mm)	t (mm)	d (mm)	b (mm)	D2 (mm)		F (Hz)	value
DL-MPP 1	0.8	0.6	6	50	0.8	0.6	6	50	0.42	456	0.82
DL-MPP 2	0.8	0.6	6	50	0.8	0.8	6	50	0.40	480	0.81
DL-MPP 3	0.8	0.6	6	50	0.8	1	6	50	0.37	484	0.75
DL-MPP 4	1	0.8	6	50	1	0.8	6	50	0.41	478	0.79
DL-MPP 5	1	0.8	6	50	0.8	0.8	6	50	0.39	484	0.80
DL-MPP 6	1	0.8	6	50	0.6	0.8	6	50	0.37	474	0.77
DL-MPP 7	0.8	0.8	10	50	0.8	0.8	2	50	0.33	412	0.89
DL-MPP 8	0.8	0.8	10	50	0.8	0.8	6	50	0.38	404	0.90
DL-MPP 9	0.8	0.8	10	50	0.8	0.8	10	50	0.43	384	0.92

The confirmation tests for the proposed model and the validation of the optimal conditions were repeated at the optimal point. The mean values from 5 experiments as well as the values predicted by the regression model and its related statistical parameters are shown in Table 9.

3.7. Comparison with the analytical model

Fig. 12 illustrates the comparison of the measured and predicted acoustic sound absorption graphs for MPP 12 made of PLA/corkwood and PLA with varying air cavity depths (i.e. 30, 50 and 70 mm). In contrast to the NFRC-MPP the measured values of PLA-MPP accord reasonably with the results from Maa's analytical model. The measured sound absorption coefficient values for the NFRC-MPP have a broader absorption bandwidth and a lower absorption peak than those predicted by Maa's model. While the resonant frequency at which the peak sound absorption coefficient occurs also agree fairly well with the data from measurement, peak sound absorption coefficient values was lower than the values predicted by the model.

Several factors contribute to the observed differences between the model predictions and the experimental outcomes: (i) the irregular and imprecise circular shape of the perforations with the lowest roundness value (Fig. 13); (ii) irregularities in the shape of the perforations due to burr formation along the edges; (iii) the bed support of the printer potentially resulting in an uneven back surface with grainy textures (Fig. 14). As presented by the Maa model, the circular perforations are expected to have a uniform and equal geometric shape. However, our samples exhibited non-circular perforations (Fig. 13), and the back surface of the samples was uneven and unpolished due to contact with the 3D printer support (Fig. 14). These aforementioned factors affect the propagation of sound waves, leading to measurement errors that the analytical model fails to consider.

It is also noteworthy that NFRC-MPP simultaneously absorbs sound energy through two mechanisms: resonance (associated with the Helmholtz absorber) and viscothermal loss (related to porous materials). As a result, Maa's model is not well-suited for accurately predicting the values of sound absorption coefficients for this type of sound absorber, typically resulting in underestimated values.

3.8. The double-layer sound absorber

According to Fig. 14, the sound absorption performance of the double layered MPPA at different frequencies was obtained through a two MPP layer structure backed by an air cavity of various depths. For this purpose, 2 MPP layers with completely identical dimensions ($t = 1$ mm, $d = 0.8$ mm, and $b = 6$ mm) were utilized.

As shown in Fig. 15, if the back cavity D2 is held constant, the value of SACA will increase with an increase in D1, and the initial peak of sound absorption will travel down in frequency. Likewise, when the air distance D1 remains constant, while the value of D2 is increasing, the value of SACA also increases, and the first sound absorption peak shifts towards lower frequencies. By simultaneously increasing the distances (depths) of the back cavities D1 and D2, the SACA value also increases and the initial absorption peak would appear within the lower frequencies as well.

In order to determine the impact of modifying the parameters of the second layer of the DL-MPP, three distinct modes with the specifications shown in Table 9 were employed. As shown in Table 10 and Fig. 16, when the perforation diameter (d) of the second layer increases, the SACA value falls, and the initial absorption peak shifts only slightly towards higher frequencies. An increase in perforation diameter (d) values in the second layer contribute to the decrease in SACA values, however, the magnitude and position of the initial absorption peak remain unaffected. Moreover, by extending the distance between the perforations (b) of the second layer, the value of SACA advances, while the value and position of the first absorption peak stay unaltered.

3.9. NFRC-MPP backed by kenaf fibre

In order to fabricate a hybrid absorber with the maximum sound absorption capability, MPP 12 (the optimized sample), and an optimal porous sound absorber (made of natural kenaf fibers) [69–71] were employed. As shown in Fig. 17, several arrangements were used to combine the kenaf layer and MPP as well as to determine the optimum combination.

Fig. 18 demonstrates that the sound absorption performance of absorbers with the MPP layer as the front layer is enhanced than those with the kenaf layer as the front layer at low frequencies. It is therefore evident that employing the MPP in conjunction with the porous kenaf sound absorber would maximize the absorption peak values and expand the absorption frequency bandwidth.

The values of D1 and D2 were tested in the MAPA sample, which showed better performance in terms of the frequency spectrum and SACA value than other arrangements (Fig. 19).

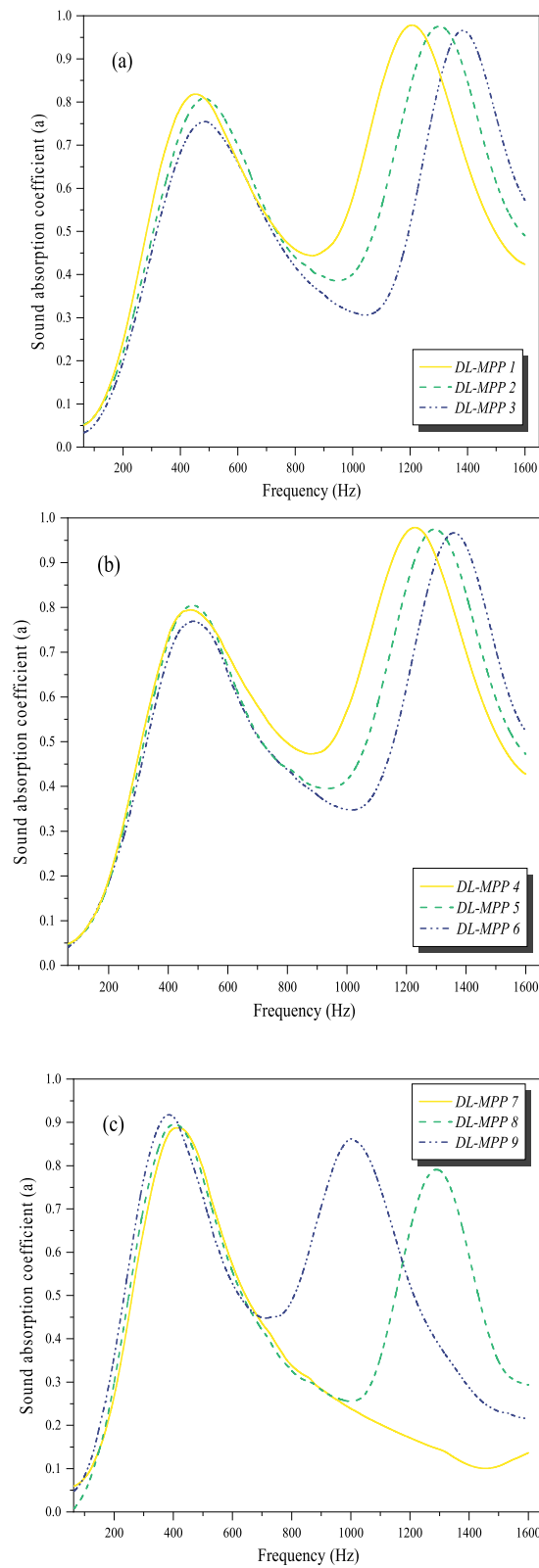


Fig. 16. The impacts of modifying the parameters of the second layer on the values of the acoustic absorption coefficient of DL-MPP sound absorbers a) increasing the diameters of the perforations (d), b) decreasing the thickness (t), c) the distance between the perforations (b).

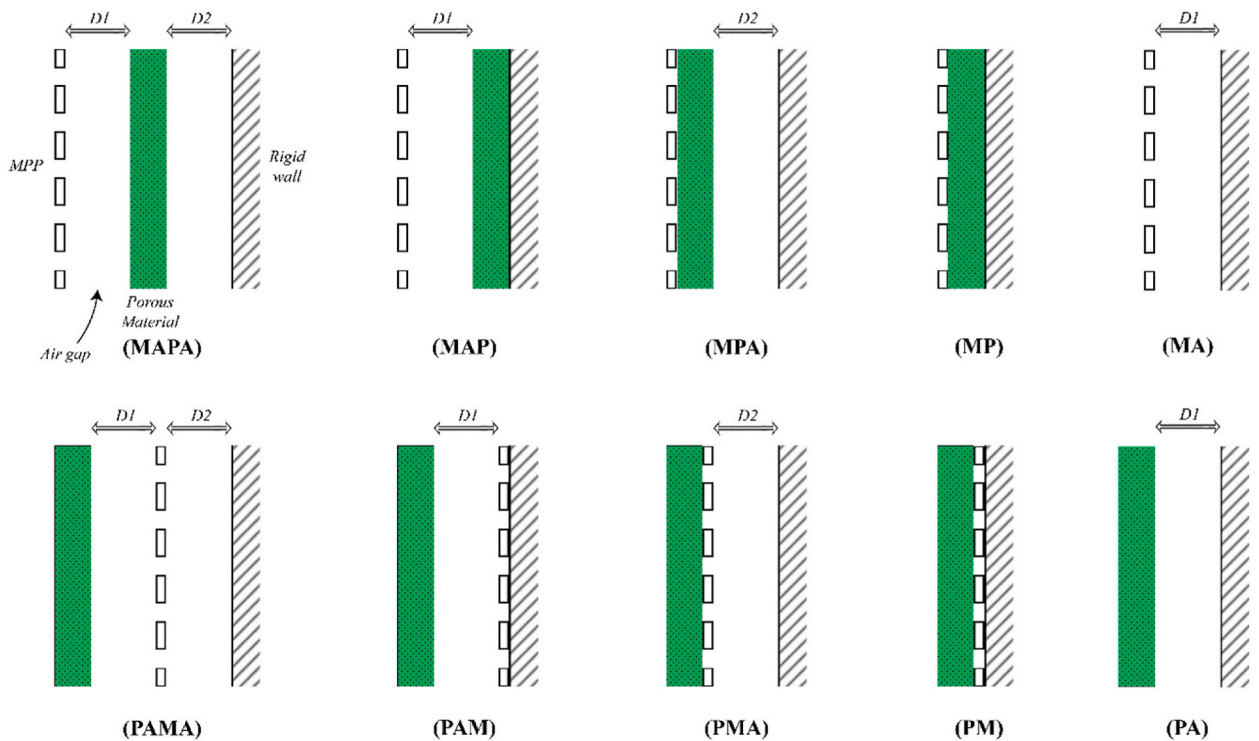


Fig. 17. Various combinations for the placement of kenaf sound absorber and MPP layer: P) Porous, A) Back cavity, M) MPP.

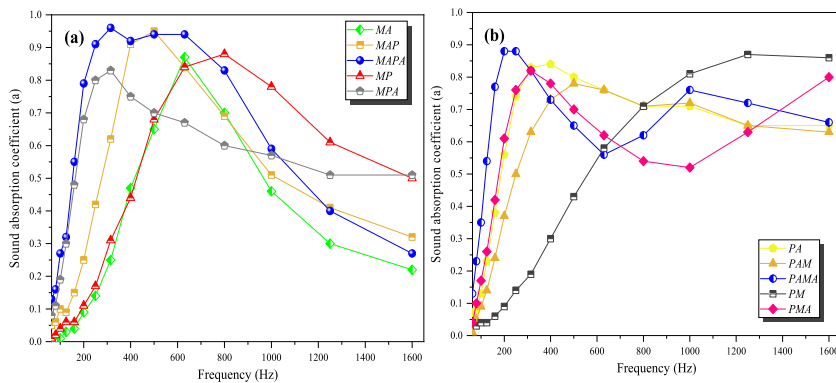


Fig. 18. Graphs depicting the sound absorption coefficient values of the double-layer sound absorbers consisting of a kenaf layer and an MPP layer A) cases where the MPP sound absorber is placed in front of the kenaf sound absorber and B) cases where the kenaf sound absorber is placed in front of the MPP sound absorber.

Fig. 20-A shows that when distance D1 is held constant, raising the value of distance D2 would contribute to expanding the sound absorption frequency bandwidth, and enhancing the values of SACA. On the other hand, raising the value of the distance D2 results in a decrease in the peak values of sound absorption and a shift towards the low frequency range where the maximum sound absorption occurs. Fig. 20-B illustrates the result of increasing distance D1 while maintaining distance D2 at a constant value. The increase in distance D1 broadens the absorption frequency bandwidth and raises the SACA values, along with increasing the absorption peak values. Additionally, the frequency with the maximum sound absorption shifts to lower frequencies as the distance D1 is increased.

Table 11, includes all the important information for manufacturing the recommended absorber. For more information about the 3D printing process and Kenaf preparation details please refer to 2.1, 2.2.

4. Conclusions

Microporous panels made of polylactic acid (PLA) polymer reinforced with corkwood fibers were successfully fabricated by 3D printing at a high manufacturing convenience and a relatively competitive prototype cost. An RSM-CCD optimization method that maximized the absorption performance and minimized the manufacturing cost was introduced for the micro perforated panels with

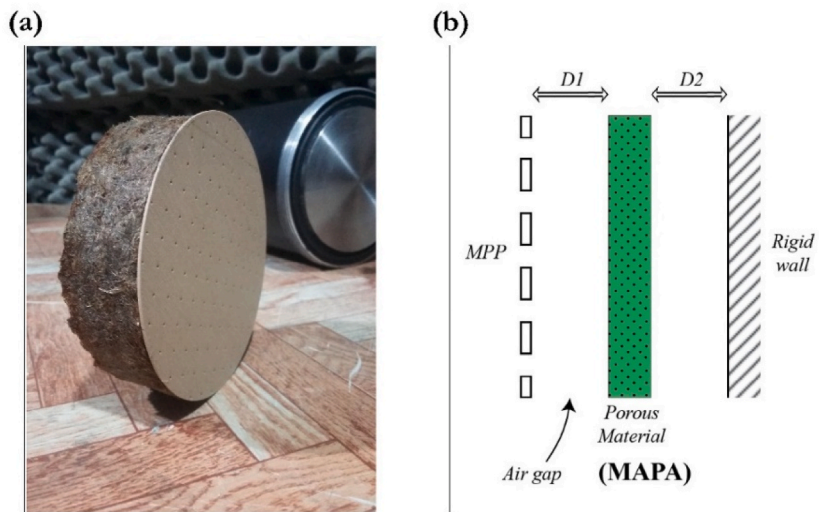


Fig. 19. a) MAPA sound absorber b) the schematic of the sound absorber.

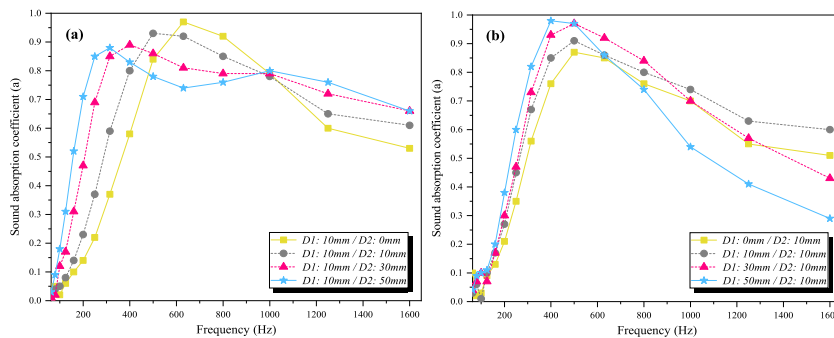


Fig. 20. Effect of back cavity depth on sound absorption performance of MAPA absorber (A: the value of D1 is constant and D2 is variable and B: the value of D1 is variable and D2 is constant).

Table 11
Detailed description of Manufacturing of MAPA.

Absorber	Material		Air Gap		Optimized Physical properties			Acoustical Properties		
	Front Layer	Back layer	D1 (mm)	D2 (mm)	Front Layer	Back layer	SACA	Peak Frequency	SACA	
MAPA	MPP	Kenaf	10	50	t (mm) : 0.9 d (mm) : 0.7 b (mm) : 0.8 p (%) : 0.6	d (mm) : 30 ρ_{bulk} (kg/m ³) : 200 ϕ (%) : 86.18 σ (N/m ⁴ .s) : 5680 α_{∞} : 1.7 Λ (μm) : 56 Λ' (μm) : 165 Average fiber diameter (mm) : 81 Average fiber density (kg/m ³) : 1400 Binding Material : 10% Polyvinyl alcohol (PVA)	0.59	315	0.88	

various structural parameters (t, d, b, σ) in target frequency ranges. Normal incident sound absorption coefficients of each panel were measured by the impedance tube method with the transfer function approach in an acoustic lab. The cost of fabricating each panel was also estimated by taking into account criteria such as filament cost, designing and printing cost, and the cost of payments for the post-processing of the printed panels in Iranian Rials in 2020. Secondly, to investigate the impact of the panels' material and their internal porosity on their sound absorption performance, a comparable panel was fabricated from PLA polymer and its sound absorption properties were compared with those of NFRC-MPP.

Additionally, Maa's analytical model was implemented in MATLAB® and used to provide predictions about the values of the sound

absorption coefficients. The corresponding outputs from the model were then compared with the experimental results. This study also investigated the impact of the combination of MPP sound absorbers and porous material as well as the parallel combination of two layers of MPPs to broaden the frequency bandwidth and magnitudes of sound absorption coefficients. The major findings of this study are provided in the following sections.

- The material with which the panel was fabricated significantly impacted its acoustic absorption performance. As the internal porosity of the sample increases, the frequency bandwidth of the sound absorption broadens and the resonance frequency decreases. NFRC-MPP performs 25 % more superior than PLA-MPP in terms of the average sound absorption coefficient.
- It is also very interesting to note that NFRC-MPP simultaneously absorbs the sound energy through two mechanisms of resonance (the associated with the Helmholtz absorber) and viscothermal loss (related to porous materials), Maa's model does not work well at predicting the values of sound absorption coefficients of this type of sound absorber and such values are typically understated by this model. We assert the imperative for forthcoming investigations to prioritize the development of an innovative model tailored for the accurate representation of absorption coefficients within porous perforated structures.
- Fabricating acoustic absorbers via 3D printing technology and advanced FDM technique allows for developing such sound absorbers more easily and quickly than employing traditional time-consuming and laborious techniques such as manual preparation and press forming.
- The results showed that changing the back cavity depths would slightly affect the resonant frequency of the MPP. Increasing the depth of the back cavity from 30 mm to 70 mm reduced the resonant frequency by more than 41 %. Hence it is necessary to select a suitable value for the back cavity depths.
- By adding a layer of kenaf porous material behind the MPP and simultaneously introducing a cavity between the two layers and a cavity behind the kenaf absorber, a significant improvement in the SACA (mainly at lower frequencies) was achieved; however, no significant change was observed for the sound absorption in the middle frequencies.
- Enhancing the bandwidth of sound absorption at low and middle frequency ranges is substantially more effective when two identical MPP layers are arranged parallel to one another.
- To achieve high-performance sound absorbers with acceptable biocompatibility, biodegradability, and cost-effectiveness, various natural fibers and manufacturing techniques have been thoroughly studied in the field of Acoustic Science. However, there remains a crucial need to advance a range of improved NFRCs (Natural Fiber Reinforced Composites) and explore additive manufacturing approaches.
- One limitation of this study lies in the exclusive consideration of the Maa model. Therefore, it is highly recommended to conduct further analyses using alternative numerical and mathematical models such as FEM (Finite Element Method) and CFD (Computational Fluid Dynamics) to obtain more comprehensive results. Additionally, it is advised to complement the study by determining absorption values experimentally through alternative methods, such as the reverberation room method and the utilization of acoustic simulation software, for a more expansive dataset.

CRediT authorship contribution statement

Ehsan Rezaeian: Resources, Methodology, Data curation. **Ebrahim Taban:** Supervision, Resources, Methodology, Conceptualization, Writing – original draft. **Umberto Berardi:** Supervision, Resources, Conceptualization. **Seyyed Bagher Mortazavi:** Writing – original draft, Data curation, Conceptualization. **Mohammad Faridan:** Project administration, Methodology, Funding acquisition. **Elham Mahmoudi:** Investigation, Formal analysis.

Declaration of competing interest

The authors declare that they have no known competing financial interests or personal relationships that could have appeared to influence the work reported in this paper.

Data availability

The authors are unable or have chosen not to specify which data has been used.

Acknowledgments

This study is funded by the Iran National Science Foundation (INSF) for the financial support of this research project [grant number 4002451

References

- [1] M. Basner, et al., Auditory and non-auditory effects of noise on health, *Lancet* 383 (9925) (Apr. 12 2014) 1325–1332, [https://doi.org/10.1016/S0140-6736\(13\)61613-X](https://doi.org/10.1016/S0140-6736(13)61613-X). Lancet Publishing Group.
- [2] T. Münzel, M. Sørensen, A. Daiber, Transportation noise pollution and cardiovascular disease, *Nat. Rev. Cardiol.* 18 (9) (Sep. 2021) 619–636, <https://doi.org/10.1038/s41569-021-00532-5>. Nature Publishing Group.
- [3] C. Magnussen, et al., Global effect of modifiable risk factors on cardiovascular disease and mortality, *N. Engl. J. Med.* 389 (14) (Oct. 2023) 1273–1285, <https://doi.org/10.1056/nejmoa2206916>.
- [4] D.A. Bies, C.H. Hansen, C.Q. Howard, K.L. Hansen, *Engineering Noise Control*, sixth ed., CRC Press, Boca Raton, 2023 <https://doi.org/10.1201/9780367814908>.

- [5] A.I. Mosa, A. Putra, R. Ramlan, A.A. Esraa, Wideband sound absorption of a double-layer microperforated panel with inhomogeneous perforation, *Appl. Acoust.* 161 (Apr. 2020) 107167, <https://doi.org/10.1016/j.apacoust.2019.107167>.
- [6] D.-Y. Maa, Theory and design of microperforated panel sound-absorbing constructions, *Sci. Sin.* 18 (1) (1975) 55–71.
- [7] F. Rañique, J. Hui Wu, C. Rui Liu, F. Ma, Transmission Loss analysis of a simple expansion chamber muffler with extended inlet and outlet combined with inhomogeneous micro-perforated panel (iMPP), *Appl. Acoust.* 194 (Jun. 2022) 108808, <https://doi.org/10.1016/j.apacoust.2022.108808>.
- [8] X. Zhang, L. Cheng, Acoustic silencing in a flow duct with micro-perforated panel liners, *Appl. Acoust.* 167 (Oct. 2020) 107382, <https://doi.org/10.1016/j.apacoust.2020.107382>.
- [9] F. Czwielong, S. Floss, M. Kaltenbacher, S. Becker, Influence of a micro-perforated duct absorber on sound emission and performance of axial fans, *Appl. Acoust.* 174 (Mar. 2021) 107746, <https://doi.org/10.1016/j.apacoust.2020.107746>.
- [10] Y. Qian, Y. Wei, D. Kong, H. Xu, Experimental investigation on motor noise reduction of Unmanned Aerial Vehicles, *Appl. Acoust.* 176 (May 2021) 107873, <https://doi.org/10.1016/j.apacoust.2020.107873>.
- [11] B. Usmonov, Investigation of the Potential of Micro Perforated Panel Absorber in Aircraft Noise Reduction, Hamburg University of Technology (TUHH), 2001.
- [12] P. Cobo, F. Simón, Multiple-layer microperforated panels as sound absorbers in buildings: a review, *Buildings* 9 (2) (Feb. 25 2019) 53, <https://doi.org/10.3390/buildings9020053>. Multidisciplinary Digital Publishing Institute (MDPI).
- [13] P. Cobo, C. de la Colina, E. Roibás-Millán, M. Chimeno, F. Simón, A wideband triple-layer microperforated panel sound absorber, *Compos. Struct.* 226 (Oct. 2019) 111226, <https://doi.org/10.1016/j.compstruct.2019.111226>.
- [14] S. Xie, D. Wang, Z. Feng, S. Yang, Sound absorption performance of microperforated honeycomb metasurface panels with a combination of multiple orifice diameters, *Appl. Acoust.* 158 (Jan. 2020) 107046, <https://doi.org/10.1016/j.apacoust.2019.107046>.
- [15] S. Ahsani, et al., Sound absorption enhancement in poro-elastic materials in the viscous regime using a mass-spring effect, *J. Sound Vib.* 511 (Oct. 2021) 116353, <https://doi.org/10.1016/j.jsv.2021.116353>.
- [16] N.A. George, P. Nassos, Practical Sustainability Strategies: How to Gain a Competitive Advantage, 2020.
- [17] Y.J. Qian, K. Cui, S.M. Liu, Z.B. Li, D.Y. Kong, S.M. Sun, Numerical study of the acoustic properties of micro-perforated panels with tapered hole, *Noise Control Eng. J.* 62 (3) (May 2014) 152–159, <https://doi.org/10.3397/1/376216>.
- [18] D.D.V.S. Chin, M.N. Bin Yahya, N. Bin Che Din, P. Ong, Acoustic properties of biodegradable composite micro-perforated panel (BC-MPP) made from kenaf fibre and polylactic acid (PLA), *Appl. Acoust.* 138 (Sep. 2018) 179–187, <https://doi.org/10.1016/j.apacoust.2018.04.009>.
- [19] J. Liu, X. Hua, D.W. Herrin, Estimation of effective parameters for microperforated panel absorbers and applications, *Appl. Acoust.* 75 (1) (Jan. 2014) 86–93, <https://doi.org/10.1016/j.apacoust.2013.07.009>.
- [20] P. Cobo, F. Montero De Espinosa, Proposal of cheap microperforated panel absorbers manufactured by infiltration, *Appl. Acoust.* 74 (9) (Sep. 2013) 1069–1075, <https://doi.org/10.1016/j.apacoust.2013.03.003>.
- [21] D. Yang, X. Wang, M. Zhu, The impact of the neck material on the sound absorption performance of Helmholtz resonators, *J. Sound Vib.* 333 (25) (Dec. 2014) 6843–6857, <https://doi.org/10.1016/j.jsv.2014.07.034>.
- [22] H. Ruiz, P. Cobo, T. Dupont, B. Martin, P. Leclaire, Acoustic properties of plates with unevenly distributed macroperforations backed by woven meshes, *J. Acoust. Soc. Am.* 132 (5) (Nov. 2012) 3138–3147, <https://doi.org/10.1121/1.4754520>.
- [23] Y.J. Qian, D.Y. Kong, S.M. Liu, S.M. Sun, Z. Zhao, Investigation on micro-perforated panel absorber with ultra-micro perforations, *Appl. Acoust.* 74 (7) (Jul. 2013) 931–935, <https://doi.org/10.1016/j.apacoust.2013.01.009>.
- [24] Z. Liu, J. Zhan, M. Fard, J.L. Davy, Acoustic measurement of a 3D printed micro-perforated panel combined with a porous material, *Measurement* 104 (Jul. 2017) 233–236, <https://doi.org/10.1016/j.measurement.2017.03.032>.
- [25] S.S. Kamble, A. Gunasekaran, S.A. Gawankar, Sustainable Industry 4.0 framework: a systematic literature review identifying the current trends and future perspectives, *Process Saf. Environ. Protect.* 117 (Jul. 2018) 408–425, <https://doi.org/10.1016/j.psep.2018.05.009>.
- [26] M.R. Khosravani, T. Reinicke, On the environmental impacts of 3D printing technology, *Appl. Mater. Today* 20 (Sep. 2020), <https://doi.org/10.1016/j.apmt.2020.100689>.
- [27] S.E. Kishore, R. Sujithra, B. Dhatey, A review on latest acoustic noise mitigation materials, *Mater. Today: Proc.* 47 (Jan. 2021) 4700–4707, <https://doi.org/10.1016/j.matpr.2021.05.600>.
- [28] J.S. Chen, Y. Bin Chen, Y.H. Cheng, L.C. Chou, A sound absorption panel containing coiled Helmholtz resonators, *Phys. Lett. Sect. A Gen. At. Solid State Phys.* 384 (35) (Dec. 2020), <https://doi.org/10.1016/j.physleta.2020.126887>.
- [29] S. Kumar, T.B. Xiang, H.P. Lee, Ventilated acoustic metamaterial window panels for simultaneous noise shielding and air circulation, *Appl. Acoust.* 159 (Feb. 2020) 107088, <https://doi.org/10.1016/j.apacoust.2019.107088>.
- [30] N. Aravantinos-Zafiris, F. Lucklum, M.M. Sigalas, Complete phononic band gaps in the 3D Yablonovite structure with spheres, *Ultrasonics* 110 (Feb. 2021) 106265, <https://doi.org/10.1016/j.ultras.2020.106265>.
- [31] L. Fang, J. Liu, S. Ju, F. Zheng, W. Dong, M. Shen, Experimental and theoretical evidence of enhanced ferromagnetism in sonochemical synthesized BiFeO₃ nanoparticles, *Appl. Phys. Lett.* 97 (24) (Dec. 2010), <https://doi.org/10.1063/1.3525573/122616>.
- [32] K.H. Matlack, A. Bauhofer, S. Krödel, A. Palermo, C. Daraio, Composite 3D-printed metastructures for low-frequency and broadband vibration absorption, *Proc. Natl. Acad. Sci. USA* 113 (30) (Jul. 2016) 8386–8390, <https://doi.org/10.1073/pnas.1600171113>.
- [33] A. Kruisová, et al., Ultrasonic bandgaps in 3D-printed periodic ceramic microlattices, *Ultrasonics* 82 (Jan. 2018) 91–100, <https://doi.org/10.1016/j.ultras.2017.07.017>.
- [34] G. do N. Almeida, E.F. Vergara, L.R. Barbosa, R. Brum, Low-frequency sound absorption of a metamaterial with symmetrical-coiled-up spaces, *Appl. Acoust.* 172 (Jan. 2021) 107593, <https://doi.org/10.1016/j.apacoust.2020.107593>.
- [35] C. Liu, B. Xia, D. Yu, The spiral-labyrinthine acoustic metamaterial by coiling up space, *Phys. Lett. Sect. A Gen. At. Solid State Phys.* 381 (36) (Sep. 2017) 3112–3118, <https://doi.org/10.1016/j.physleta.2017.07.041>.
- [36] X. Man, T. Liu, B. Xia, Z. Luo, L. Xie, J. Liu, Space-coiling fractal metamaterial with multi-bandgaps on subwavelength scale, *J. Sound Vib.* 423 (Jun. 2018) 322–339, <https://doi.org/10.1016/j.jsv.2018.02.060>.
- [37] L. Yuvaraj, S. Jeyanthi, L.B. Mailan Chinnappandi, J. Pitchaimani, Experimental and numerical investigation on sound absorption characteristics of 3D printed coupled-cavity integrated passive element systems, *J. Low Freq. Noise Vib. Act. Control* 41 (1) (Mar. 2022) 60–73, <https://doi.org/10.1177/14613484211042157>.
- [38] V. Sekar, S.Y. Eh Noum, S. Sivanesan, A. Putra, D.D. Chin Vui Sheng, D.H. Kassim, Effect of thickness and infill density on acoustic performance of 3D printed panels made of natural fiber reinforced composites, *J. Nat. Fibers* 19 (13) (Dec. 2022) 7132–7140, <https://doi.org/10.1080/15440478.2021.1944426>.
- [39] A.R. Kshirsagar, D. Job Sandeep Rajprian, J. Jeyanthi, Design and development of acoustic metamaterial and micro-perforated panel by using 3D printing, in: *Lecture Notes in Mechanical Engineering*, Springer, Singapore, 2021, pp. 501–510, https://doi.org/10.1007/978-981-16-1769-0_45.
- [40] M.R. Khosravani, T. Reinicke, Experimental characterization of 3D-printed sound absorber, *Eur. J. Mech. Solid.* 89 (Aug. 2021) 104304, <https://doi.org/10.1016/j.euromechsol.2021.104304>.
- [41] M. Askari, et al., Additive manufacturing of metamaterials: a review, *Addit. Manuf.* 36 (Dec. 2020) 101562, <https://doi.org/10.1016/j.addma.2020.101562>.
- [42] T.D. Ngo, A. Kashani, G. Imbalzano, K.T.Q. Nguyen, D. Hui, Additive manufacturing (3D printing): a review of materials, methods, applications and challenges, *Compos. B Eng.* 143 (Jun. 15 2018) 172–196, <https://doi.org/10.1016/j.compositesb.2018.02.012>. Elsevier Ltd.
- [43] J. Boulvert, et al., Acoustic modeling of micro-lattices obtained by additive manufacturing, *Appl. Acoust.* 164 (Jul. 2020) 107244, <https://doi.org/10.1016/j.apacoust.2020.107244>.
- [44] V. Sekar, M.H. Fouladi, S.N. Namasivayam, S. Sivanesan, Additive manufacturing: a novel method for developing an acoustic panel made of natural fiber-reinforced composites with enhanced mechanical and acoustical properties, *J. Eng.* 2019 (Sep. 2019) 1–19, <https://doi.org/10.1155/2019/4546863>.
- [45] D. Stooß, K. Pickering, Y. Zhang, Fused deposition modelling of natural fibre/poly(lactic acid) composites, *J. Compos. Sci.* 1 (1) (Aug. 2017) 8, <https://doi.org/10.3390/jcs1010008>.

- [46] V. Sekar, et al., Effect of perforation volume on acoustic absorption of the 3D printed micro-perforated panels made of polylactic acid reinforced with wood fibers, *J. Phys. Conf.* 2120 (1) (Dec. 2021) 012039, <https://doi.org/10.1088/1742-6596/2120/1/012039>.
- [47] B. Crawford, et al., Effect of fungal deterioration on physical and mechanical properties of hemp and flax natural fiber composites, *Materials* 10 (11) (Oct. 2017) 1252, <https://doi.org/10.3390/ma10111252>.
- [48] B. Tisserat, Z. Liu, V. Finkenstadt, B. Lewandowski, S. Ott, L. Reifschneider, 3D printing biocomposites, *Plast. Res. Online* (2015) 1–3, <https://doi.org/10.2417/spepro.005690>.
- [49] N.K. Kim, S. Dutta, D. Bhattacharyya, A review of flammability of natural fibre reinforced polymeric composites, *Compos. Sci. Technol.* 162 (Jul. 7 2018) 64–78, <https://doi.org/10.1016/j.compscitech.2018.04.016>. Elsevier.
- [50] S. Knapic, V. Oliveira, J.S. Machado, H. Pereira, Cork as a building material: a review, *Eur. J. Wood Wood Prod.* 74 (6) (Nov. 2016) 775–791, <https://doi.org/10.1007/s00107-016-1076-4>.
- [51] E.M. Fernandes, V.M. Correlo, J.A.M. Chagas, J.F. Mano, R.L. Reis, Properties of new cork-polymer composites: advantages and drawbacks as compared with commercially available fibreboard materials, *Compos. Struct.* 93 (12) (Jun. 2011) 3120–3129, <https://doi.org/10.1016/j.compstruct.2011.06.020>.
- [52] V. Mazzanti, L. Malagutti, F. Mollica, FDM 3D printing of polymers containing natural fillers: a review of their mechanical properties, *Polymers* 11 (7) (Jun. 2019) 1094, <https://doi.org/10.3390/polym11071094>.
- [53] ZORTRAX.COM, Zortrax M200. <https://zortrax.com/3d-printers/m200/>.
- [54] E. Rezaieyan, E. Taban, S.B. Mortazavi, A. Khavanin, H. Asilian, E. Mahmoudeh, Acoustic properties of 3D printed bio-degradable micro-perforated panels made of Corkwood Fiber-Reinforced composites, *J. Heal. Saf. Work* 12 (2) (2022) 367–383 [Online]. Available: <http://jhsw.tums.ac.ir/article-1-6689-en.html>. (Accessed 22 November 2023).
- [55] E. Taban, S. Amininasab, P. Soltani, U. Berardi, D.D. Abdi, S.E. Samaei, Use of date palm waste fibers as sound absorption material, *J. Build. Eng.* 41 (Sep. 2021) 102752, <https://doi.org/10.1016/j.jobe.2021.102752>.
- [56] D.-Y. Maa, Potential of microperforated panel absorber, *J. Acoust. Soc. Am.* 104 (5) (Nov. 1998) 2861–2866, <https://doi.org/10.1121/1.423870>.
- [57] D.Y. Maa, Microperforated-panel wideband absorbers, *Noise Control Eng. J.* 29 (3) (1987) 77–84, <https://doi.org/10.3397/1.2827694>.
- [58] Y.-S. Wong, V. Sekar, S.Y. Eh Noum, S. Sivanesan, Effect of thickness and perforation size on the acoustic absorption performance of a micro-perforated panel, *MATEC Web Conf* 335 (Jan. 2021) 03016, <https://doi.org/10.1051/mateconf/202133503016>.
- [59] K. Sakagami, M. Morimoto, M. Yairi, A. Minemura, A pilot study on improving the absorptivity of a thick microperforated panel absorber, *Appl. Acoust.* 69 (2) (Feb. 2008) 179–182, <https://doi.org/10.1016/j.apacoust.2006.09.008>.
- [60] Z. Liu, J. Zhan, M. Fard, J.L. Davy, Acoustic properties of multilayer sound absorbers with a 3D printed micro-perforated panel, *Appl. Acoust.* 121 (Jun. 2017) 25–32, <https://doi.org/10.1016/j.apacoust.2017.01.032>.
- [61] E. Taban, et al., Morphological, acoustical, mechanical and thermal properties of sustainable green Yucca (*Y. gloriosa*) fibers: an exploratory investigation, *J. Environ. Heal. Sci. Eng.* 18 (2) (Dec. 2020) 883–896, <https://doi.org/10.1007/s40201-020-00513-9>.
- [62] M. Hajimohammadi, P. Soltani, D. Semnani, E. Taban, H. Fashandi, Nonwoven fabric coated with core-shell and hollow nanofiber membranes for efficient sound absorption in buildings, *Build. Environ.* 213 (Apr. 2022) 108887, <https://doi.org/10.1016/j.buildenv.2022.108887>.
- [63] D.D. Chin Vui Sheng, M.N. Bin Yahya, N. Bin Che Din, Sound absorption of microperforated panel made from coconut fiber and polylactic acid composite, *J. Nat. Fibers* 19 (7) (Jul. 2022) 2719–2729, <https://doi.org/10.1080/15440478.2020.1821290>.
- [64] X. Wang, et al., The interfacial shear strength of carbon nanotube sheet modified carbon fiber composites, *Conf. Proc. Soc. Exp. Mech. Ser.* (2021) 25–32, https://doi.org/10.1007/978-3-030-59542-5_4/COVER.
- [65] D. Cao, et al., The effect of resin uptake on the flexural properties of compression molded sandwich composites, *Wind Energy* 25 (1) (Jan. 2022) 71–93, <https://doi.org/10.1002/WE.2661>.
- [66] D. Cao, S. Malakooti, V.N. Kulkarni, Y. Ren, H. Lu, Nanoindentation measurement of core-skin interphase viscoelastic properties in a sandwich glass composite, *Mech. Time-Dependent Mater.* 25 (3) (Sep. 2021) 353–363, <https://doi.org/10.1007/S11043-020-09448-Y/METRICS>.
- [67] J. Wong, et al., Triplet fusion upconversion for photocuring 3D-printed particle-reinforced composite networks, *Adv. Mater.* 35 (11) (Mar. 2023) 2207673, <https://doi.org/10.1002/ADMA.202207673>.
- [68] M. Alizadeh-Osgouei, Y. Li, C. Wen, A comprehensive review of biodegradable synthetic polymer-ceramic composites and their manufacture for biomedical applications, *Bioact. Mater.* 4 (1) (Dec. 1 2019) 22–36, <https://doi.org/10.1016/j.bioactmat.2018.11.003>. Elsevier.
- [69] E. Taban, et al., Measurement, modeling, and optimization of sound absorption performance of Kenaf fibers for building applications, *Build. Environ.* 180 (Aug. 2020) 107087, <https://doi.org/10.1016/j.buildenv.2020.107087>.
- [70] B.Y. Yun, H.M. Cho, Y.U. Kim, S.C. Lee, U. Berardi, S. Kim, Circular reutilization of coffee waste for sound absorbing panels: a perspective on material recycling, *Environ. Res.* 18 (2020) 109281.
- [71] S. Ehsan, U. Berardi, E. Taban, P. Soltani, S. Mohammad Mousavi, Natural fibro-granular composite as a novel sustainable sound-absorbing material, *Appl. Acoust.* 181 (2021) 108157, <https://doi.org/10.1016/j.apacoust.2021.108157>.